FACTS and Synchronous Condensers in High-PV Power Systems: A Comparative Technical Review

LEESHEN PATHER, RUDIREN SARMA
Discipline of Electrical, Electronic and Computer Engineering, University of KwaZulu-Natal
Mazisi Kunene Road, Glenwood, Durban 4041
SOUTH AFRICA

Abstract: - High penetration of photovoltaic (PV) generation reduces system strength and introduces voltage control, power quality, and transfer capacity constraints across transmission and distribution networks. This review comparatively examines the operating principles, control mechanisms, dynamic response, and deployment implications of key FACTS devices that include: TCSC, TSSC, SVC, STATCOM and SSSC together with Synchronous Condensers. The comparison is organized around a common analytical perspective comprising reactive-power controllability, response speed, voltage support capability, short-circuit contribution, oscillation damping, and practical implementation considerations. The review shows that converter-based shunt devices provide very fast reactive current support and effective voltage regulation but contribute to limited fault current and may require harmonic mitigation; series controllers primarily enhance transfer capability and damping through manipulation of line reactance or injected series voltage. Synchronous Condensers remain particularly valuable where inertia, fault-level support and strong grid behaviour are required, although with higher losses, larger footprint and greater maintenance burden. On this basis, the paper provides technically grounded guidance on matching device type to grid need and on the coordinated deployment of electronic and rotating compensation in high-PV systems.

Key-Words: - FACTS, STATCOM, SVC, SSSC, TCSC, Synchronous Condenser, reactive power, system strength, power quality.

Received: March 11, 2026. Revised: May 10, 2026. Accepted: June 13, 2026. Published: September 14, 2026.

1 Introduction

The energy landscape has undergone rapid transformation, driven by several key disruptors. One of the most significant issues is the increasing penetration of large-scale photovoltaic (PV) systems into the transmission networks. This shift is part of the broader global transition from conventional coal-fired power generation toward cleaner renewable energy sources. As a result, the energy system is evolving in terms of the generation mix, operational dynamics, and infrastructure requirements [1]. Many countries worldwide rely on coal-fired power stations because of the availability of resources. However, this is a diminishing resource, with many countries having only a few decades of coal reserves available based on the current consumption patterns. As an example, South Africa, ranked among the top ten countries globally in coal reserves, holds an estimated 31 Gt in reserve, with a usage of 284 Mt/Yr as per a study conducted in 2020. [2].

Global warming has had catastrophic long-term impacts on the climate. Countries around the world have collaborated to put forward various initiatives to reduce carbon emissions, which are the prime drivers of global warming. The use of renewable energy sources for power generation is one of the key drivers towards meeting global zero emission targets. In 2023, owing to the introduction of several non-renewable energy sources, the impact of an increase in emissions was lessened [2], [3]. There has been a global shift toward renewable energy sources, with solar power emerging as the most prevalent, owing to the massive amount of energy received from the sun [4]. In the United States, the solar industry added a substantial 50 GWdc of new solar generation capacity, representing a 21% increase from 2023 to 2024, accounting for 66% of all new generating capacity introduced in 2024, as depicted in Figure 1 [5]. Similarly, South Africa has demonstrated significant growth in both solar photovoltaic and concentrated solar power (CSP), with the installed capacity increasing from 960 MW in 2014 to 2,787 MW by 2025, as illustrated in Figure 2. Photovoltaic systems offer numerous advantages, including improved generation efficiency, reduced maintenance requirements and minimal environmental impacts. These benefits have led to a rapid increase in large-scale PV deployment. However, this accelerated growth presents challenges related to the quality and stability of the power systems. Understanding these impacts is crucial for mitigating potential issues and ensuring a reliable energy future [6], [7], [8].

This paper is not intended merely as a device comparison tutorial. Its principal contribution is a unified comparative framework that positions series FACTS devices, shunt FACTS devices, and Synchronous Condensers within the context of high-PV power systems. The comparison is developed around six system relevant attributes: reactive-power controllability, dynamic response speed, voltage support effectiveness, oscillation damping capability, short-circuit contribution and practical implementation burden. Standard equations and machine relationships are restated only where necessary to establish a consistent analytical basis for comparison. The originality of the paper therefore lies in the technology integration, the integrated interpretation of the governing control channels and the practical selection guidance derived from the cited literature rather than in reproducing textbook derivations in isolation.

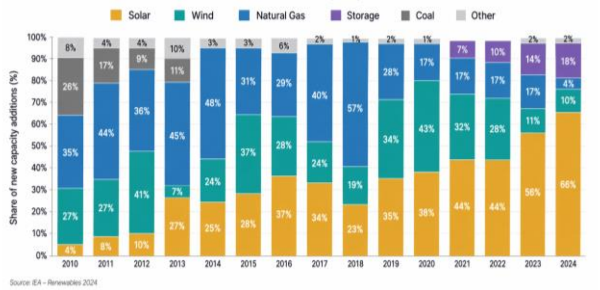

Fig. 1: US Electricity Generation Profile between 2010 & 2024

Source: created by the authors based on [5].

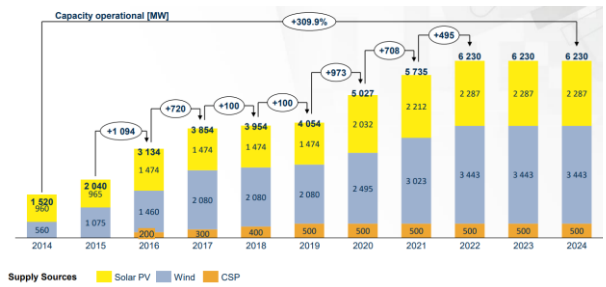

Fig. 2: RSA Solar PV, Wind & CSP Production

Source: created by the authors based on [6].

For clarity, no figures or tables in this manuscript are reproduced directly from the authors' prior publications. Standard equations and classical analytical relationships are restated in the authors' own comparative narrative solely to establish a common technical basis for review. Where concepts, device characteristics, or analytical formulations follow established literature, the relevant sources are explicitly cited.

2 Quality of Supply

2.1 Voltage Regulation

Photovoltaic plants can introduce voltage fluctuations and regulation challenges, primarily because of the rapid changes in solar irradiance caused by passing cloud cover. These irradiance variations lead to intermittent power output, which is typically observed at the Point of Common Coupling (PCC). Consequently, the voltage at the PCC can fluctuate significantly, potentially disrupting the performance of the voltage regulation equipment and negatively affecting the operation of associated control systems. The integration of photovoltaic systems can exacerbate voltage imbalance in power distribution networks. This imbalance is commonly quantified using the Voltage Unbalance Factor (VUF), as represented in Equation 1, where V^{-} is the negative-sequence voltage component and V^{+} is the positive-sequence voltage component. Several utilities have established acceptable VUF limits. For example, in Malaysia, the benchmark is typically set at 2%. VUF tends to be directly proportional to the power output of the PV plant, meaning that higher PV generation can lead to greater voltage imbalance [9], [10].

$$VUF = \frac{V^{-}}{V^{+}} X\ 100 (1)$$

2.2 Harmonics

One of the main issues introduced by inverter-based PV systems is the generation of harmonic components, which cause harmonic distortions that adversely affect electrical equipment and degrade the power quality of the distribution grid. Studies have shown that the harmonic distortion of the current is inversely proportional to solar irradiance, indicating that more harmonics are injected into the system when it operates at lower power levels. A study conducted in Brazil assessed the impact of photovoltaic integration on a distribution system using the IEEE 37-bus test feeder. This study focused on evaluating the Total Harmonic Distortion (THD) levels in voltage and current, based on Equation 2, where $THD_v$is the total harmonic distortion in voltage, v_h is the RMS voltage of the h^{th} harmonic, v_1 is the RMS voltage of the fundamental frequency, $h$is the harmonic order starting from 2 and $h =$ maxis the maximum harmonic order considered in Equation 3, where THD_i is the total harmonic distortion in current, i_h is the RMS current of the h^{th} harmonic, i_1 is the

RMS current of the fundamental frequency, h is the harmonic order starting from 2 and $h =$ maxis the maximum harmonic order considered. The findings indicated that the most significant voltage distortions and harmonic currents were observed in the 3rd, 5th, and 7th harmonic components. It was also found that current harmonics pose substantial risks to the system's stability and performance. As PV penetration increases, these harmonic distortions may intensify, underscoring the necessity of implementing harmonic filters to mitigate their adverse effects efficiently [11].

$$THDv = \sqrt{\sum_{h=2}^{h=max} \frac{v_{h^2}}{v_{1^2}}}\ x\ 100(2)$$

$$THDi = \sqrt{\sum_{h=2}^{h=max} \frac{i_{h^2}}{i_{1^2}}}\ x\ 100(3)$$

2.3 Short Circuit Fault Level Contribution

Inverter-based PV plants generally contribute limited fault current because converter controls enforce strict current limits. In practice, the injected fault current is typically only modestly above rated current (often around 1.2–1.5 pu. for grid-following PV, depending on vendor and grid code settings), so their contribution to system short-circuit level is much smaller than that of synchronous machines [12], [13].

An inverter-based source under balanced conditions is modelled as a voltage source integrated into a system via a Thevenin equivalent, as shown in Figure 3. If a single line to ground fault is experienced in phase a, as shown in Figure 4, the following Equations apply (Equations 4 to 6). The positive, negative and zero-sequence short-circuit currents (SCCs) are derived by interconnecting the respective sequence networks, forming a composite network that reflects the system's response under asymmetrical fault conditions, as depicted in Equation 6, where I_f^+ is the positive-sequence fault current, V_a is the pre-fault voltage at phase A, Z_{af} is the impedance between phase A and the fault point, I_{af} is the fault current in phase a, I_{bf} is the fault current in phase b, I_{cf} is the fault current in phase c, z^0, z^-, z^+ zero, negative, and positive sequence impedances, respectively [14], [15].

$$I_{bf} = I_{cf} = 0(4)$$
$$V_{ag} = Z_{af} I_{af}(5)$$
$$I_f^+ = \frac{V_a}{(3Z_af + z^0 + z^- + z^+)} = \frac{V_a}{Z_af}(6)$$

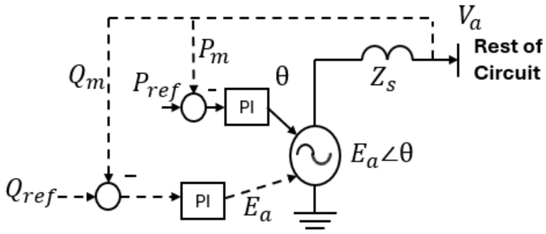

Fig. 3: Voltage Source via Thevenin's Circuit
Source: created by the authors based on [14], [15].

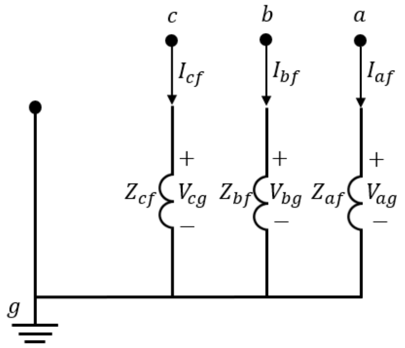

Fig. 4: General 3 Phase Bus
Source: created by the authors based on [14], [15].

2.4 Reactive Power Support

The integration of photovoltaic sources into power systems significantly increases the demand for reactive power support. This is primarily due to the inherent inability of most PV systems, particularly those interfaced through inverters, to supply reactive power under standard operating conditions. The switching of integrated capacitor banks and the operation of load tap changers (LTCs) in response to voltage rises or dips caused by photovoltaic generation can lead to reactive power fluctuations. These fluctuations affect both the distribution and transmission systems. At high levels of PV penetration, this becomes particularly substantial, and the need to manage the reactive power across a broader network has increased. As supplying reactive power from a transmission system is typically more expensive than managing it locally within the distribution network, this dynamic can result in substantial economic impacts [11], [16].

Effective control of the power flow in an AC transmission line is essential to enhance the power transfer capacity and ensure system stability, particularly in response to system disturbances. The stability of an electric power system can be compromised by various factors, including frequency deviations, power oscillations, voltage collapse, and loss of synchronism. These phenomena can lead to cascading failures if not promptly and adequately addressed. Therefore, implementing control strategies and technologies that allow for real-time modulation of power flows is critical for maintaining operational reliability and avoiding widespread outages [17].

The power flow is represented by Equation 7, where P is the active power transmitted, V_1, V_2 are the sending and receiving voltage magnitudes, X is the reactance of the transmission line, $\theta_1 - \theta_2$ is the phase angle difference between the sending and receiving voltages, and the maximum power transfer over a transmission line is governed by Equation 8, where the angle δ_{max} represents the maximum allowable angle difference to maintain the system stability, which is determined based on the stiffness of the terminal buses and the desired stability margins. This power transfer limit, P_{max} is typically constrained by transient or steady-state stability considerations rather than the thermal capacity of the conductor. Consequently, P_{max} is often less than the thermal limit defined by the current-carrying capability of line conductors [17].

$$P = \frac{V_1 V_2}{X} \sin(\theta_1 - \theta_2) (7)$$
$$P_{max} = \frac{V_1 V_2}{X} sin\delta_{max} (8)$$

The introduction of series compensation using series capacitor banks increases the maximum power transfer capability of transmission lines. This is because the effective reactance of the line is reduced by the capacitive reactance, X_c introduced by the capacitor banks, as described in Equation 9, where X is the original transmission line reactance and k_{se} represents the degree of series compensation. A lower total reactance leads to an increase in P_{max}, enhancing the power transfer efficiency of the line [11].

$$X_c = X(1 - k_{se}) (9)$$

Thyristor-Controlled Series Compensation (TCSC) is an advanced form of compensation. It utilizes thyristor-controlled reactors (TCRs) connected in parallel with fixed series capacitors to adjust the effective compensating reactance X_c. This dynamic control capability helps mitigate subsynchronous resonance (SSR), a phenomenon that can destabilize the torsional modes of turbine generators, particularly in steam power stations transmitting energy over series-compensated lines [17].

Power flow in relatively short transmission lines can be controlled using a phase shifting transformer (PST), which introduces a phase angle shift via a complex turns ratio of unit magnitude, which is represented by Equation 10, where ϕ represents the phase shift introduced by the PST, V_1 is the sending-end voltage magnitude, V_2 is the receiving-end voltage magnitude, X is the transmission-line reactance and θ is the phase-angle difference between the sending and receiving voltages. However, under dynamic conditions, PSTs respond too slowly to become effective. In contrast, thyristor-based switching devices offer fast and discrete control of the phase angle ϕ, enabling more responsive power flow management. Additionally, the maximum transferable power P_{max} can be increased by regulating the input voltage to the AC line. Owing to this ability, voltage V_2 changes as the load changes and is represented by Equation 11, where $\theta_1$and θ_2 are the sending and receiving end voltage angles, respectively. When substituted into Equation 10, Equation 12 is derived, where δ_{max} is the maximum allowable power angle. As shown in Equation 12, the dynamic reactive power support at bus 2 (as illustrated in Figure 5) enables the regulation of the bus voltage by compensating for voltage drops and maintaining voltage stability under varying load conditions. This is achieved using a controllable reactive power source, where Q_c represents the reactive power injected at the receiving end of the AC line, as represented in Figure 5 and shown in Equation 13 [17].

Equations 7 to 13 establish the common analytical pathway used throughout the remainder of this review. From a system perspective, power transfer can be improved by reducing the effective series reactance, by increasing the controlled bus voltage, or by coordinating both actions. Series devices such as the TCSC, TSSC and SSSC therefore act primarily through the ΔX channel, whereas shunt devices such as the SVC, STATCOM and Synchronous Condenser act primarily through the ΔQ–ΔV channel. This distinction is important because it explains why series compensation is especially effective for transfer capacity enhancement and oscillation damping, while shunt compensation is more directly associated with voltage regulation, reactive power reserve and post-disturbance voltage recovery. Mechanically switched devices can support the steady-state operating point, but rapid stability support requires controllers with sufficiently fast dynamic response [17], [18].

$$P_{max} = \frac{V_1 V_2}{X} \sin((\theta_1 - \theta_2) \pm \emptyset) (10)$$
$$V_2 = V_1 \, cos(\theta_1 - \theta_2) \; (11)$$
$$P_{max} = \frac{{V_1}^2 \, sin2\delta_{max}}{2X} \; (12)$$
$$Q_c = \frac{{V_2}^2 - V_1 V_2 \cos(\theta_1 - \theta_2)}{X} \; (13)$$

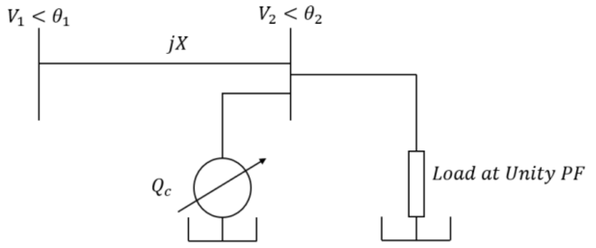

Fig. 5: Transmission Line Compensated By a Controllable Reactive Power Source

Source: created by the authors based on [17].

Frequent faults in both transmission and distribution systems remain persistent challenges for global utilities. In many cases, these systems lack sufficient fault ride-through capabilities, leading to operational disruptions. Major disturbances can cause generator rotors to oscillate, resulting in power fluctuations across transmission lines. Even if the system withstands an initial fault, transient stability becomes a critical concern during the post-fault restoration phase. One of the primary challenges in this period is managing the fluctuating reactive power demand or addressing the inadequate reactive power support. These fluctuations can lead to voltage instability, which compromises overall system reliability [18].

Significant increases in transmission line loading can lead to voltage collapse, primarily owing to inadequate reactive power support at load centers. This deficiency is often caused by reactive power-consuming loads, such as those in induction motors. The reactive power, voltage and current exchanged between reactive components, inductors and capacitors are expressed by Equation 14 to Equation 18, where Q represents the reactive power, I the current through the reactive element, X the reactance, V_s the source voltage, $V_L(\omega t)$ the instantaneous voltage across the inductor at time t, $I_L(\omega t)$ instantaneous current through the conductor at time t, V_M the peak voltage across the inductor, I_M the peak current through the inductor, ω the angular frequency, $P_L(\omega t)$ the instantaneous power across the inductor at time t, the instantaneous power across the capacitor at time t, V_{rms} the root mean square value of voltage ($V_{\text{rms}} = \frac{V_m}{\sqrt{2}}$), I_{rms} the root mean square value of current $\left(I_{\text{rms}} = \frac{I_m}{\sqrt{2}}\right)$, $V_C(\omega t)$ instantaneous voltage across the capacitor at time t, $I_C(\omega t)$ instantaneous current across the capacitor at time t [19].

$$Q = I^2 X = \frac{{V_s}^2}{X} VAR (14)$$

$$V_L(\omega t) = V_M \sin(\omega t + 90°)\,;$$
$$I_L(\omega t) = I_M \sin(\omega t) (15)$$

$$P_L(\omega t) = V_L(\omega t) I_L(\omega t) = \frac{V_M}{\sqrt{2}} \cdot \frac{I_M}{\sqrt{2}} \sin(2\omega t)$$
$$= V_{\text{rms}} I_{\text{rms}} \sin(2\omega t) (16)$$

$$V_C(\omega t) = V_M \sin(\omega t - 90°)\,;$$
$$I_C(\omega t) = I_M \, sin(\omega t) \quad (17)$$

$$P_C(\omega t) = V_C(\omega t) I_C(\omega t) = \frac{-V_M}{\sqrt{2}} \cdot \frac{I_M}{\sqrt{2}} \sin(2\omega t) = -V_{\text{rms}} I_{\text{rms}} \sin(2\omega t) (18)$$

The reactive power for an inductive load supplied by the single-phase AC source is shown in Figure 6. As shown, no net energy was consumed over a complete cycle. The energy is alternately stored and released by the inductor's magnetic field, resulting in a continuous exchange of energy between the source and the inductor.

However, the capacitive load depicted in Figure 7 demonstrates a condition in which the current leads the voltage. This behaviour reflects the capacitor's tendency to store energy in its electric field and subsequently return it to the source without any net energy consumption over the entire cycle. The complex power in an AC circuit can be determined using the Equations below, where S is the complex power, $|\,S\,|$ is the apparent power magnitude, $P$the real power, $Q$the reactive power, j the imaginary unit, V the RMS voltage, I the RMS current, Z the impedance magnitude, $V\angle\theta_v$ the voltage phasor with magnitude V and phase angle θ_v, $I\angle-\theta_I$ the complex conjugate of the current phasor, θ_v the voltage phase angle, θ_I the current phase angle, Re{·} the real part of a complex quantity and Im{·} the imaginary part of a complex quantity, which express both the active (real) and reactive components [19].

$$S = P + jQ (19)$$

$$|S| = VI = I^2 \,|\, Z \,|\, = \frac{V^2}{|Z|} \text{VA} (20)$$

$$S = VI^* = (V\angle\theta_V)(I\angle-\theta_I) = VI\cos(\theta_V - \theta_I)$$
$$+ jVI \sin(\theta_V - \theta_I) (21)$$

$$P = \text{Re}[S] = VI\cos(\theta_v - \theta_I) = |S|\cos\phi \text{ W}\,;$$
$$Q = \text{Im}[S] = VI\sin(\theta_v - \theta_I) = |S|\sin\phi \text{ VAR} (22)$$

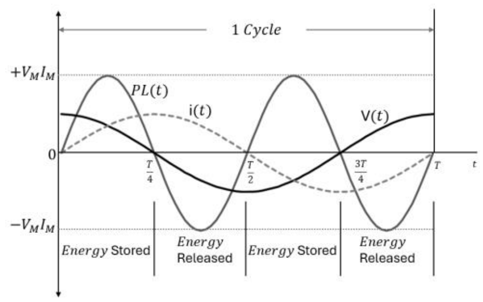

Fig. 6: Inductive Load

Source: created by the authors based on [19].

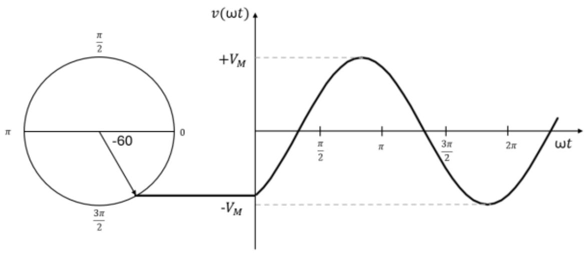

Fig. 7: Capacitive Load

Source: created by the authors based on [19].

3 FACTS Devices

3.1 Background

The integration of advanced technologies, such as Flexible AC Transmission Systems and Synchronous Condensers, has proven effective in mitigating some of the issues raised in previous paragraphs. These devices provide dynamic reactive power compensation, enhance voltage control, and contribute to the overall stability of the power system. Their implementation facilitates increased power transfer capabilities, defers the need for extensive infrastructure upgrades, and minimizes environmental impact. Additionally, they enable utilities to maximize the throughput and operational efficiency of existing power networks, while maintaining system reliability and stability [18].

FACTS is a collection of power electronic-based devices used in alternating current systems to enhance controllability and increase power transfer capabilities. These controllers can be classified into four categories: shunt-connected controllers, series-connected controllers, combined series-series controllers, and combined shunt-series controllers. These can be used to adjust several parameters (voltage, current, impedance, or phase angle), which in turn improve the power flow, voltage regulation, reduce system losses, transient stability, and oscillation of the system [17].

FACTS controllers typically operate under three main control schemes: steady-state power flow control, transient stability control, and power oscillation damping. These devices employ operational strategies such as line impedance modulation, voltage regulation and load flow management, with each type tailored to specific system requirements. For shunt FACTS controllers, the focus is on the STATCOMs and SVCs, which are primarily used for voltage regulation. These devices provide reactive power compensation and maintain bus voltage stability [20], [21], [22].

In series-connected FACTS controllers, the primary focus is on three key devices: Thyristor-Switched Series Capacitor (TSSC), Thyristor-Controlled Series Capacitor (TCSC), and Static Synchronous Series Compensator (SSSC). These devices are utilized to enhance the power transfer capability, improve system stability, and provide dynamic control of the line impedance in transmission networks [23].

Series compensation has historically been the most practical method for mitigating the effects of series inductance in transmission lines, thereby enhancing power transfer capability. However, this approach has several limitations. One of the primary concerns is the introduction of resonant frequencies below the fundamental power frequency owing to the insertion of the series capacitors. These capacitors can interact with both the generator and line inductances, resulting in sub-harmonic resonances [23].

Such resonances can be excited by transient disturbances and may lead to a range of adverse phenomena, including

1. Self-excitation of synchronous generators.
2. Rotor hunting (sustained rotor angle oscillations).
3. Torsional (shaft) oscillations can compromise the mechanical integrity of turbine generator shafts [23].

3.2 Thyristor-Switched Series Capacitor (TCSC)

Compensation for a transmission line's series reactance can be resolved using combinations of fixed-series capacitors and TCSC banks. A TCSC typically consists of a fixed series capacitor and a thyristor-controlled reactor parallel to the capacitor, as depicted in Fig. 1, where V_c represents the voltage across the TCSC, I_L is the power frequency line current, I_c is the current through the series capacitor, I_{TH} is the current through the bidirectional thyristor valve [24]. The thyristor-switched capacitor TCSC operates in three primary modes.

1. In bypass mode, the thyristors conduct fully, and the reactor bypasses the capacitor (low and zero compensation).
2. Blocked mode, in which the thyristors are blocked and only the capacitor remains in the circuit, providing fixed capacitive compensation.
3. Partially conducting modes in which the thyristors are phase controlled (variable compensation, which can be capacitive or reactive) [24].

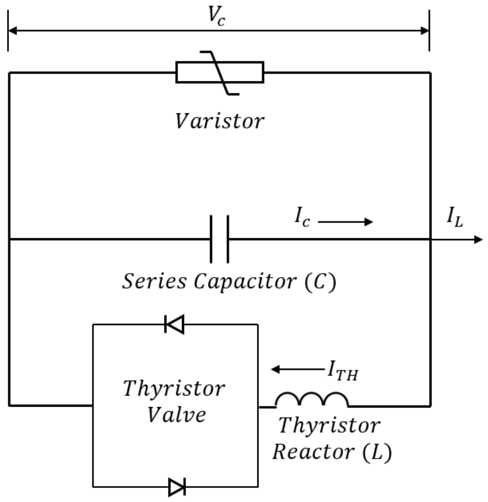

Fig. 8: TCSC Circuit (Controllable Subsegment)
Source: created by the authors based on [24].

Table 1 and Figure 9 summarize the increase in distortion as the effective reactance is raised through thyristor control. Figure 10 and Figure 11 show the steady-state waveforms of the basic (TSC) circuit operating in the capacitive region. The capacitor voltage waveform is shown for different control angles (= 180° and 145°), where α denotes the control angle, defined as the electrical angle from the zero-crossing of the capacitor voltage to the point at which the thyristor begins conduction. The conduction interval, represented by σ, is symmetric about the zero crossing of . The thyristor current () lags behind the capacitor voltage, highlighting the inherent phase relationship between the current and Table 1. VariationsSource: compiled by the authors based on [24], [25].X Power Frequency RMS Voltage (pu.)Power Frequency Peak Voltage (pu.)Total RMS Voltage (pu.)Thyristor ActionEffect111.4141No thyristor action (fully bypassed or fixed cap).System behaves ideally (pure sinusoid).222.562.02Partial conduction through thyristor.The effective capacitive reactance is increased above the nominal value and harmonic content becomes noticeable owing to partial thyristor conduction 333.393.03More aggressive conduction (smaller firing angle).The effective capacitive reactance is further increased above the nominal value and the waveform becomes markedly non-sinusoidal owing to asymmetrical thyristor conduction.Table 1. VariationsSource: compiled by the authors based on [24], [25].X Power Frequency RMS Voltage (pu.)Power Frequency Peak Voltage (pu.)Total RMS Voltage (pu.)Thyristor ActionEffect111.4141No thyristor action (fully bypassed or fixed cap).System behaves ideally (pure sinusoid).222.562.02Partial conduction through thyristor.The effective capacitive reactance is increased above the nominal value and harmonic content becomes noticeable owing to partial thyristor

3.2 Thyristor-Switched Series Capacitor (TCSC)

Compensation for a transmission line's series reactance can be resolved using combinations of fixed-series capacitors and TCSC banks. A TCSC typically consists of a fixed series capacitor and a thyristor-controlled reactor parallel to the capacitor, as depicted in Fig. 1, where V_c represents the voltage across the TCSC, I_L is the power frequency line current, I_c is the current through the series capacitor, I_{TH} is the current through the bidirectional thyristor valve [24]. The thyristor-switched capacitor TCSC operates in three primary modes.

- In bypass mode, the thyristors conduct fully, and the reactor bypasses the capacitor (low and zero compensation).
- Blocked mode, in which the thyristors are blocked and only the capacitor remains in the circuit, providing fixed capacitive compensation.
- Partially conducting modes in which the thyristors are phase controlled (variable compensation, which can be capacitive or reactive) [24].

Table 1. X_{ORDER} Variations

X	Power Frequency RMS Voltage (pu.)	Power Frequency Peak Voltage (pu.)	Total RMS Voltage (pu.)	Thyristor Action	Effect
1	1	1.414	1	No thyristor action (fully bypassed or fixed cap).	System behaves ideally (pure sinusoid).
2	2	2.56	2.02	Partial conduction through thyristor.	The effective capacitive reactance is increased above the nominal value and harmonic content becomes noticeable owing to partial thyristor conduction
3	3	3.39	3.03	More aggressive conduction (smaller firing angle).	The effective capacitive reactance is further increased above the nominal value and the waveform becomes markedly non-sinusoidal owing to asymmetrical thyristor conduction.

Source: compiled by the authors based on [24], [25].

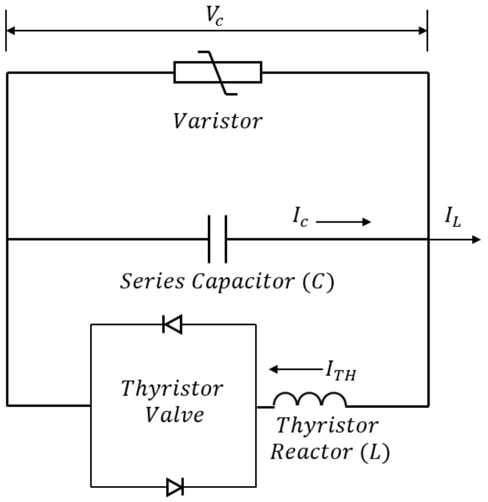

Fig. 1: TCSC Circuit (Controllable Subsegment). Source: created by the authors based on [24].

Table 1 and Figure 9 summarize the increase in distortion as the effective reactance is raised through thyristor control. Fig. 3 and Fig. 4 show the steady-state waveforms of the basic (TSC) circuit operating in the capacitive region. The capacitor voltage waveform is shown for different control angles (α = 180° and 145°), where α denotes the control angle, defined as the electrical angle from the zero-crossing of the capacitor voltage V_c to the point at which the thyristor begins conduction. The conduction interval, represented by σ, is symmetric about the zero crossing of V_c. The thyristor current (I_{TH}) lags behind the capacitor voltage, highlighting the inherent phase relationship between the current and voltage in a capacitive switching operation [24], [25]. Figure 11 shows that when a subsegment operates in capacitive mode, current in the thyristor branch increases the power frequency voltage across the capacitor segment, thereby increasing the effective capacitive reactance, as expressed in Equation 23, where X_{eff} is the effective reactance, X_α is the net reactance under thyristor control at the firing angle α and X_c is the nominal capacitor reactance. This produces an effective reactance greater than the nominal value, with X_{ORDER} representing the ratio of X_α to X_c, as indicated in Equation 24. Equation 25 gives the relationship between peak and root mean square voltage, where V_{peak} is the peak voltage and V_{RMS} is the root-mean-square voltage. However, the thyristor branch current also distorts the capacitor voltage waveform, introducing non-fundamental frequency components and harmonics so that the waveform departs from a pure sinusoid.

Table 1 provides a standardized reference for comparing the resulting waveform degradation. Accordingly, Figure 11 and Table 1 should be interpreted together, since they illustrate the fundamental trade off governing practical TCSC operation: as the firing angle is reduced from the blocked condition, thyristor-branch conduction increases, the effective capacitive boost across the segment becomes larger and both the RMS and peak capacitor segment voltages rise above their nominal values, thereby strengthening the apparent series capacitive compensation seen by the line. At the same time, the waveform becomes progressively less sinusoidal, indicating increasing distortion. Thus, the results show that stronger controllability is achieved together with greater waveform distortion, meaning that the practical TCSC operating point must be selected by balancing the required degree of series compensation against harmonic performance, resonance avoidance, and acceptable capacitor segment stress [24], [25].

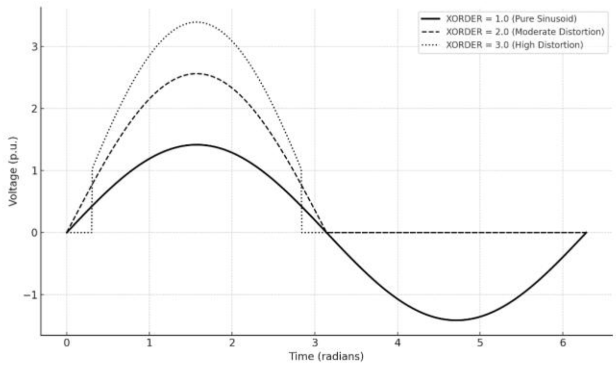

Fig. 2: Voltage Waveform Distortion at Different X_{ORDER} Values.
Source: created by the authors based on [24], [25].

$$X_{eff} = X_\alpha > X_C \tag{23}$$

$$X_{ORDER} = \frac{X_\alpha}{X_C} \tag{24}$$

$$V_{peak} = \sqrt{2} V_{RMS} \tag{25}$$

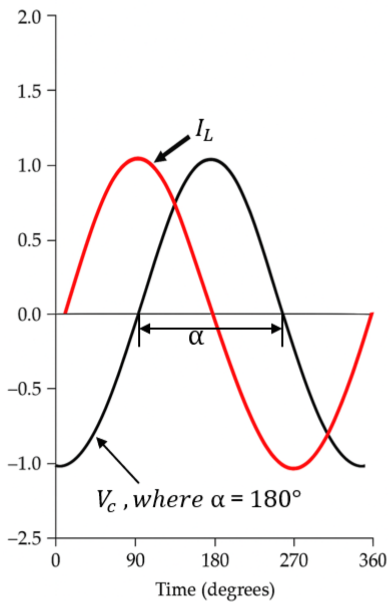

Fig. 3: Steady State Wave Form (Capacitive Range, X Order = 1).
Source: created by the authors based on [24], [25].

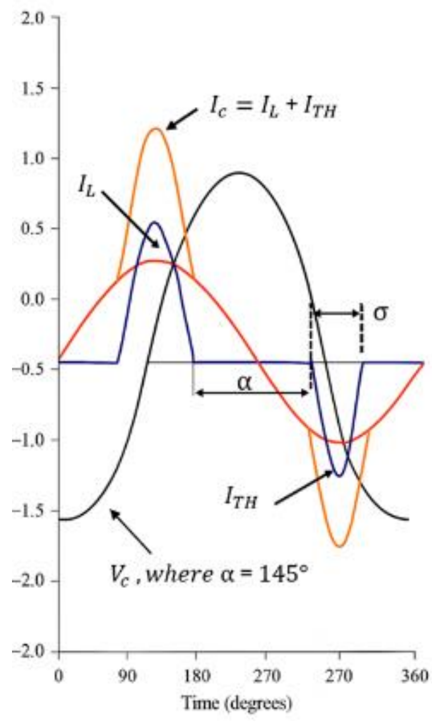

Fig. 4: Steady State Wave Form (Capacitive Range, X Order = 2).
Source: created by the authors based on [24], [25].

Equation 26 methodically defines the equivalent capacitive reactance of a Thyristor-Controlled Series Capacitor operating in the capacitive region as a function of the thyristor firing angle, α. The expression incorporates contributions from the nominal capacitive reactance, fundamental frequency component, and harmonic distortion effects introduced by the thyristor switching.

In this context:

- $X(\alpha)$ represents the effective (complex) series reactance at firing angle α.
- ω is the angular frequency of the power system.
- C is the capacitance of the series capacitor.
- j is the imaginary unit, indicating capacitive reactance.
- k denotes the ratio of the natural resonant frequency to the system frequency ($\lambda/\omega k$).
- λ is the natural frequency of the LC circuit.
- L is the inductance of the thyristor-controlled reactor.
- α is the firing angle of the thyristor and
- σ = 2(π−α) is the thyristor conduction angle per half cycle.

Equation 26 shows that the TCSC is not simply a fixed series capacitor with an adjustable switch. It is a dynamic impedance controller whose effective reactance depends on the firing angle and on the resonant interaction between the fixed capacitor and the thyristor-controlled reactor. Accordingly, variation of the firing angle modifies the apparent line reactance seen by the network and therefore shifts the power flow operating point, the synchronizing torque, and the damping characteristics of the corridor. This is why the TCSC is particularly effective when the dominant planning objective is power flow redistribution or oscillation damping rather than direct local voltage support or fault-level reinforcement [24], [25].

By controlling $X(\alpha)$ the TCSC enables real-time modulation of the transmission line reactance, which is critical for power flow control, oscillation damping, transient stability enhancement, and transmission capacity increase [24], [25].

$$X(\alpha) = \frac{-j}{\omega C}\left[1 - \frac{k^2}{k^2-1}\cdot\frac{\sigma+\sin(\sigma)}{\pi} + \frac{4k^2}{k^2-1}\cdot\cos^2\left(\frac{\sigma}{2}\right)\cdot\frac{k\tan\left(\frac{k\sigma}{2}\right)-\tan\left(\frac{\sigma}{2}\right)}{\pi}\right] \quad (26)$$

Fig. 5 illustrates the operating characteristics of a TCSC and the relationship between the voltage across the capacitor and line current. The diagram depicts the transitions between capacitive and inductive operating modes, which are governed by the firing angle of the thyristors. In the upper right region, the TCSC functions in capacitive mode, where it behaves like a capacitor and injects leading reactive power into the system. The maximum capacitive output occurs at a firing angle of 180° when the thyristors are fully blocked, and no current flows through them; this condition corresponds to the maximum capacitive compensation point shown in Figure 12. When operating in the inductive region, the thyristors are in a conducting state, and the TCSC behaves as an inductor and absorbs reactive power. The dotted curve in this region represents the bypass operation of the TCSC, denoted X_B [25].

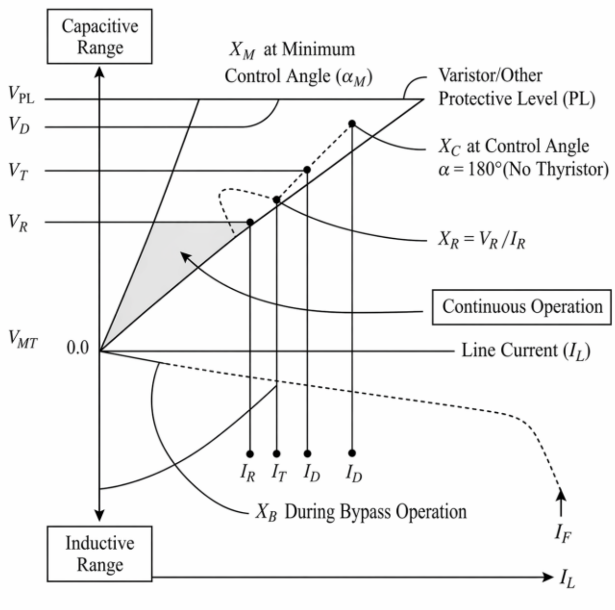

Fig. 5: Operating Characteristics of TCSC.
Source: created by the authors based on [19], [25].

3.3 The Thyristor Switched Series Capacitor (TSSC)

A Thyristor Switched Series Capacitor (TSSC) is a type of discretely controlled series compensation device employed in power transmission systems to enhance the power flow and voltage stability. It comprises multiple fixed capacitor segments connected in series with the transmission line. The total capacitance of the circuit is represented by Equation 27, where C_T represents the total capacitance, C_{TSSC} is the series capacitance, and m is the number of active capacitors. The insertion or bypassing of each capacitor segment is governed by thyristor valve pairs, which function as high-speed solid-state switches [26].

TSSC operates in discrete compensation steps:

1. When the thyristors are in the non-conduction (off) state, the corresponding capacitor segment remains inserted in the line, providing capacitive reactance and reducing effective line impedance.
2. When the thyristors are in the conduction (on) state, they provide a low-impedance path, thereby bypassing the capacitor segment ($C_T = 0$).

To mitigate the transient overvoltage and inrush currents during switching events, the firing of the thyristors was synchronized with the zero crossings of the line current. This ensures that the switching action occurs at the natural current zero points, which results in a reduction in the electromagnetic interference and mechanical stress on the system. The switching behavior and synchronization strategy are illustrated in Figure 13, where V_m represents the generator's terminal voltage, L_m is the equivalent generator inductance, R_m is the generator's internal resistance, $(T_1 - T_2, \ldots, T_n - T_{n+1})$ represent thyristors [25].

To achieve effective power factor correction and thereby maximize the active power output, the capacitive reactance of the system must be tuned to cancel out the inductive reactance. This condition ensures that the reactive power exchange is minimized, thereby enabling an optimal power transfer. This requirement is mathematically expressed in Equation 28, which defines the total capacitance necessary to fully compensate for the system's inductive reactance, where ω is the angular frequency, L is the inductance, X_C is the capacitive reactance and X_L is the inductive reactance, ensuring that the desired levels of compensation are achieved [25].

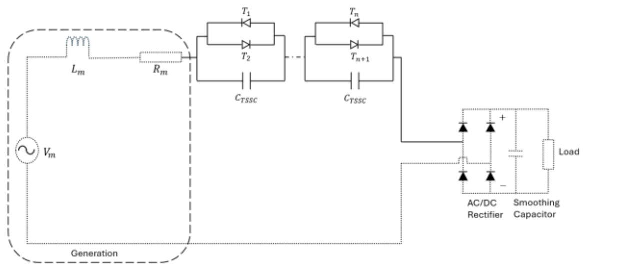

Fig. 13: TSSC Main Circuit
Source: created by the authors based on [25].

$$C_T = \frac{C_{TSSC}}{m} \quad (27)$$

$$\frac{1}{\omega C_T} = \omega L (X_C = X_L), C_T = \frac{1}{\omega^2 L} \quad (28)$$

From Figure 14, it is evident that just before the interval $\frac{3T}{2}$, where the line current crosses zero, the capacitor is inserted into the circuit to minimize switching transients. This precise insertion ensures smooth commutation. The introduction of a capacitor alters the current path owing to additional capacitive reactance. As illustrated by the highlighted waveform, the capacitor charges during the positive half-cycle and discharges during the subsequent negative half-cycle.

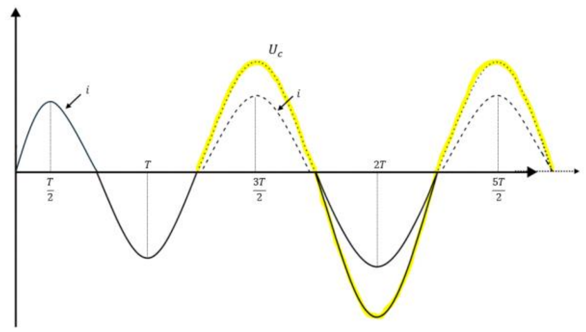

Fig. 14: Insertion of the Capacitor at the Zero Voltage Crossing

Source: created by the authors based on [25].

3.4 Static Synchronous Series Compensator (SSSC)

An alternative voltage-sourced series compensator is the static synchronous series compensator (SSSC), which is a device used to control the power flow and improve the stability of the power system by injecting a controllable voltage in series with the line. The SSSC functions by injecting a voltage in quadrature with the line current, which can behave as capacitive or inductive depending on the polarity. This may increase or decrease the overall line impedance and alter the power flow across the transmission line, as depicted in Figure 15 [25], [27]. SSSC also provides several additional benefits, including the following [28]:

1. The SSSC can be used for power factor correction, as it injects a controllable voltage in quadrature with the line current and therefore can correct the power factor when paired with the appropriate control system.
2. It can resolve unbalanced issues of active and reactive loads in both transmission and distribution systems, which in turn regulates the voltage.
3. An SSSC can also provide reactive power support, as it can supply or absorb both capacitive and inductive power, as required by the system, which aids voltage regulation.
4. The phase and magnitude of the injected voltage can be controlled using an SSSC, which allows dynamic power flow control.
5. An SSSC with an appropriate converter-based design can enable the SSSC to be used as an active filter to effectively reduce harmonic distortion and improve power quality.

The Static Synchronous Series Compensator (SSSC) operates under two principal control modes, as illustrated in Figure 15. The first mode corresponds to constant voltage compensation, where the SSSC is regulated to inject a fixed magnitude quadrature voltage into the transmission line irrespective of variations in the line current, as represented by Equation 29, where V_q is the injected voltage, I is the line current, and Q is the reactive power. In this mode, the injected reactive power was directly proportional to the magnitude of the line current. Consequently, at lower current levels, the reactive power injection was minimal, whereas at higher current levels, it increased in proportion. However, this control strategy inherently results in nonconstant reactance compensation as the equivalent reactance X, as depicted by Equation 30 [29].

$$Q = V_q I (29)$$
$$X = \frac{V_q}{I} (30)$$

The second mode of operation of the Static Synchronous Series Compensator corresponds to constant reactance compensation, in which the device maintains a fixed compensation reactance regardless of variations in the line current. In this mode, the SSSC dynamically adjusts its injected quadrature voltage, V_q, such that it remains proportional to the line current, I, as shown in Equation 31. This ensures that the overall series impedance introduced by the SSSC remains constant, which is essential for precise and stable power flow control. Under these conditions, the Transmitted power is governed by Equation 32, where P_q is the transmitted active power, V_r and V_s are the respective source voltages, X_L is the inductive reactance of the transmission line, X_{eff} is the effective reactance of the transmission line between its two ends, including the emulated variable reactance inserted by the injected voltage source of the SSSC with compensating reactance X_q, Q_q is the reactive power and δ is the power-angle difference between the terminal voltages. However, this control strategy is constrained by the voltage handling capability of the SSSC voltage-source converter. At high line current levels, the required compensation voltage may exceed the voltage rating of the converter, thereby limiting the ability to maintain full compensation [29].

$$V_q = I X_q (31)$$
$$P_q = \frac{V_s V_r}{X_{eff}} \sin(\delta) = \frac{V_s V_r}{(X_L 1 - \frac{X_q}{X_L})} \sin(\delta) (32)$$
$$Q_q = \frac{V_s V_r}{X_{eff}} \cos(1 - \delta) =$$

$$\frac{V_s V_r}{(X_L 1-\frac{X_q}{X_L})}(1-\cos(\delta)) \quad (33)$$

From Figure 15, it can be observed that the SSSC emulates a variable reactance X_q by injecting a voltage V_q, as represented by Equation 34, where I is the line current, $|X_q|$ is the magnitude of the compensating reactance and $e^{\pm j90^\circ}$ denotes a quadrature phase shift of $\pm 90°$. This voltage is orthogonal to the line current, meaning that it does not exchange real power with the system, but only reactive power. It is also observed that the positive sign in $e^{\pm j90^\circ}$ implies capacitive compensation and the negative sign implies inductive compensation. It can also be noted that the total voltage drop across the transmission line is represented by Equation 35, where V_s is the sending-end voltage, V_r is the receiving-end voltage, X_L is the inductive reactance of the transmission line, j is the imaginary unit and V_q increases or decreases the effective line reactance [30], [31], [32]:

1. If V_q opposes $jX_\mathrm{L}I$ the net reactance will decrease, resulting in increased power flow (capacitive mode).
2. If V_q aids $jX_\mathrm{L}I$ the net reactance increase decreases the power flow (inductive mode).

$$V_q = |X_\mathrm{q}| \cdot I \cdot e^{\pm j90} (34)$$
$$V_\mathrm{s} = V_\mathrm{r} + \mathrm{j}X_\mathrm{L}I + V_{\vec{q}} (35)$$

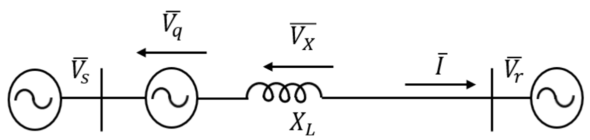

Fig. 15: Transmission line model including a Static Synchronous Series Compensator
Source: created by the authors based on [25], [27].

Figure 16 shows the operating diagram of an SSSC in terms of the injected voltageV_q, which displays the operating range of the SSSC according to various voltage and current limitations. At a lower current, a higher voltage range can be injected, as opposed to when there is a higher current, where the voltage is limited by the converter rating.

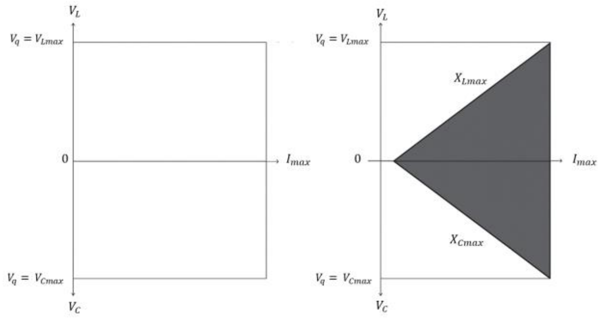

Fig. 16: Operating Diagram of a n SSSC
Source: created by the authors based on [30].

3.5 Static Var Compensator (SVC)

The most widely deployed shunt-connected FACTS devices include the Static Var Compensator (SVC), Thyristor-Controlled Reactor (TCR), and Static Synchronous Compensator (STATCOM), which are primarily utilized for dynamic reactive power compensation and voltage regulation [20], [33], [34].

A Static VAR Compensator (SVC) enhances power system stability by dynamically regulating the bus voltage magnitude by varying its output to exchange capacitive or inductive currents. It is typically comprised of thyristor-switched capacitors (TSC) and thyristor-controlled reactors (TCR). Through coordinated control of the TSC and TCR elements, the SVC modulates its reactive power (VAR) output in real time, thereby maintaining the voltage profiles and supporting the transient and dynamic voltage stability under varying load conditions. SVCs have a rapid reaction response and minimal contribution to short-circuit power, while maintaining very low maintenance [33], [34].

As illustrated in Figure 17, an SVC can improve transmission performance by strengthening voltage profiles in weak systems, reducing long-distance reactive-power transfer, supporting voltage and power oscillation damping, and delaying network reinforcement where transfer capability is constrained. In distribution applications, the same device can stabilize feeder voltage, reduce the reactive-power burden seen by the upstream source, support load balancing, and mitigate flicker and related power quality disturbances [17], [18], [25], [34], [35], [36], [37].

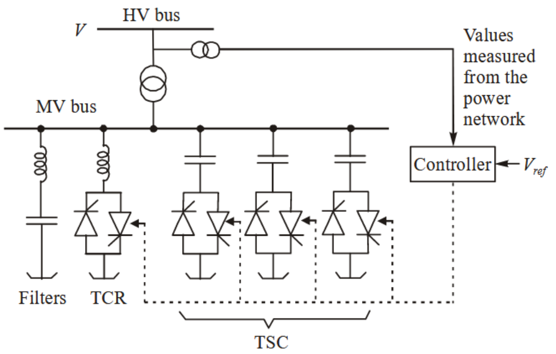

Fig. 17: Simplified Static Var Compensator
Source: created by the authors based on [34].

Figure 17 illustrates a Static Var Compensator (SVC) system composed of several key components.

Thyristor-Controlled Reactor (TCR):

- TCR controls the inductive reactance through thyristor switching. When L=0, the thyristors were blocked (no conduction). When *L*=*L*max, the thyristors are fully conducting, allowing maximum inductive current to flow. This enables smooth, continuous control of the reactive power on the inductive side.

Thyristor-Switched Capacitors (TSC):

- These are discrete capacitor banks that switch in or out by using thyristors. TSCs provide stepwise capacitive reactive power compensation and operate in conjunction with TCR.

Fixed Filters:

- These are used to filter out the low-order harmonics produced by TCR. In addition, the capacitors that make up the filters produce reactive power.

By dynamically controlling the TCR and switching TSC banks, the SVC can operate over a continuous control range of reactive power between the maximum inductive and capacitive limits. This allows the SVC to absorb or inject reactive power into the system as needed [34].

Anti-parallel thyristors were connected in pairs to enable conduction during both positive and negative halves of the AC voltage waveform. Each thyristor in the pair must either remain in conduction or be triggered at the beginning of each half-cycle to maintain continuous current flow through the capacitor or reactor. If the gate trigger signal is interrupted, the conducting thyristor will not immediately cease conducting. Instead, it continues conducting until the current naturally reaches zero at the voltage zero-crossing point. Only at this point can the other thyristor in the pair be triggered to conduct the subsequent half-cycle [34].

The TCR consists of an inductance L and a directional thyristor valve, as depicted in Figure 18. A directional valve is a specialized power electronic device that controls the flow of current and its respective direction. The valve may consist of several series-connected thyristors to achieve the desired voltage-level blocking. Thyristors 1 and 2 are operated sequentially, and one thyristor must be blocked before the other enters conduction [34].

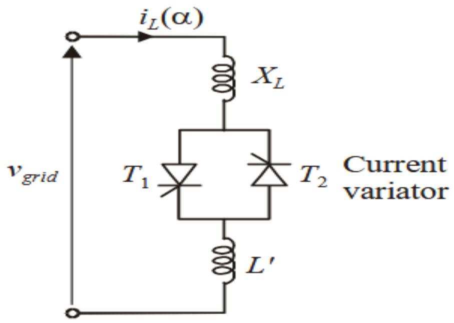

Fig. 18: Thyristor Controlled Reactor
Source: created by the authors based on [34].

The reactor current in a TCR can be dynamically regulated between maximum conduction and zero by adjusting the firing delay angle (α). This method involves delaying the firing of thyristors within each half-cycle of the AC waveform.

As shown in Figure 19 and Figure 20, the conduction period of the thyristors was determined by the chosen firing angle α. The effective current through the reactor $i_L(\alpha)$ was altered by delaying the triggering instant within the half-cycle.

- If the thyristor is fired at the zero crossing of the AC voltage waveform, it conducts for the entire half-cycle, resulting in the maximum reactor current.
- If the firing angle is increased, the thyristor conducts for a shorter duration, reducing the current through the reactor (minimum conduction when $\alpha = 180^\circ$).

At a firing angle of $\alpha = 90^\circ$ or greater (depending on the circuit conditions), no conduction may occur, and the current is effectively zero, which leads to an operational limit of ($\frac{\pi}{2} \leq \alpha \leq \pi$).

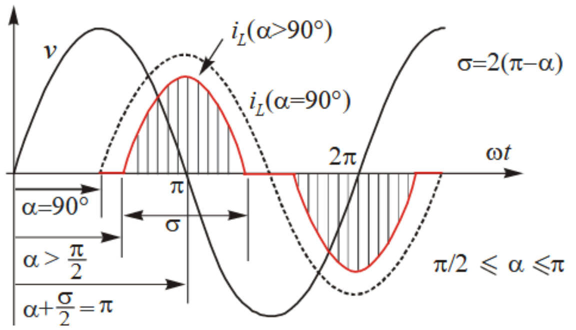

Fig. 19: Voltage & Current Waveform ( )
Source: [34].

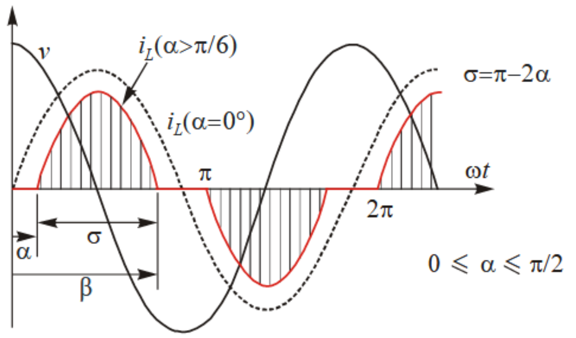

Fig. 20: Voltage & Current Waveform ()
Source: [34].

The current through the TCR can be derived by analyzing the circuit in relation to the instantaneous AC voltage and firing angle control applied to the thyristors.

There are two cases, respectively,

Case 1: $\alpha > \frac{\pi}{2}$

Conduction Period:

$$\sigma = 2\pi - 2\alpha \quad (36)$$

For case 1, the reactor current becomes discontinuous; within each half-cycle, conduction starts at α and ceases before the voltage zero-crossing, leaving an interval with zero current.

The other thyristor (for the negative half-cycle) can be fired at:

$$\alpha + \pi (37)$$

Case 2: $\alpha < \frac{\pi}{2}$

In this case, the current would not be interrupted before the next thyristor was fired at α + π leading to the current flowing in only one direction.

For normal operation, the interruption angle β must satisfy Equation 38, where σ is the conduction period and β is the interruption angle:

$$\beta < \alpha + \pi \quad (38)$$

Given that:

$$\beta = \sigma + \alpha = 2\pi - \alpha$$

Substituting:

$$2\pi - \alpha < \alpha + \pi$$

Simplifying:

$$2\pi - \alpha < \alpha + \pi \Rightarrow \pi < 2\alpha \Rightarrow \alpha > \frac{\pi}{2}$$

As shown in Figure 19 and Figure 20, the instantaneous voltage across the reactor served as the input for calculating the current waveform. Based on this analysis, the instantaneous voltage is represented by Equation 39, while the current in the circuit is represented by Equations 40 and 41, where $v(t)$ is the instantaneous voltage at time t, V is the RMS voltage, L is the inductance, $\frac{di}{dt}$ is the rate of change of current through the inductor, $i(t)$ is the instantaneous current through the inductor, ω is the angular frequency and C is the integration constant.

$$v(t) = \sqrt{2}V cos\omega t (39)$$

$$L\frac{d_i}{d_t} = \sqrt{2}V cos\omega t (40)$$

$$i(t) = \frac{\sqrt{2}V}{\omega L} sin\omega t + C (41)$$

The constant in C Equation (41) can be evaluated by considering the conditions at the instant when the thyristor becomes nonconductive, where C represents the integration constant, α is the initial phase angle, V is the RMS voltage, ω is the angular frequency, and L is the inductance. This occurs at a specific firing delay angle α, which is measured relative to the maximum input voltage waveform. Therefore, the constant can be represented as per Equation 42 below: A new Equation representing the current is depicted in Equation 43 after substituting Equation 42, where $i(t)$ is the instantaneous current through the inductor at time t, β is the end of the interval and σ is the duration of current conduction. At the instance where $\omega t = \beta$, the current in the reactor crosses zero, resulting in Equation 44 [34].

$$C = \frac{-\sqrt{2}V}{\omega L} sin\alpha (42)$$

$$i(t) = \frac{\sqrt{2}V}{X_L}(sin\omega t - sin\alpha),$$

$$\alpha < \omega t < \beta (= \alpha + \sigma) (43)$$

$$0 = \frac{\sqrt{2}V}{X_L}(sin\beta - sin\alpha) (44)$$

$$sin\beta = sin\alpha \ (45)$$

$$\alpha < \beta (= \alpha + \sigma) (46)$$

$$\beta = \pi - \alpha (47)$$

Conduction period σ is:

$$\sigma = \pi - \alpha - \alpha = \pi - 2\alpha (48)$$

3.6 Static Synchronous Compensator (STATCOM)

A Static Synchronous Compensator (STATCOM) is a shunt-connected device used to regulate the voltage in a transmission system by injecting or absorbing reactive power, which in turn improves the dynamic stability of the power system. The STATCOM is typically designed using a Voltage Source Converter (VSC) topology, which is implemented using series-connected transformers with varying control modes [40].

Relative to thyristor-based shunt compensation, the STATCOM offers very fast control response, effective reactive-current support under depressed-voltage conditions, a comparatively compact physical footprint, and inherently bidirectional reactive-power operation. These features make it particularly suitable for weak grid applications, rapid bus voltage regulation, and dynamic support during fast network disturbances. The corresponding limitations are the higher converter-related capital cost, switching and conduction losses, control-system complexity, and the need to manage converter-generated harmonics where filtering is inadequate [17], [25], [35], [36], [39].

The reactive power exchange between the STATCOM and AC systems is governed by the voltage magnitude differential between the inverter output and the system voltage. The AC voltage magnitude of the inverter is controlled by regulating the DC-link capacitor voltage. An increase in the DC capacitor voltage causes the STATCOM to operate in capacitive mode, thereby injecting reactive power into the system. Conversely, a decrease in the DC voltage results in inductive operation, where the STATCOM absorbs reactive power from the system. The real power transfer between the AC system and DC link compensates for the STATCOM losses and is regulated by the phase-angle difference between the inverter voltage and the system voltage [40].

As shown in the operating diagram in Figure 21, the voltage of the bus (V_{bus}) is equal to the summation of the voltage across the STATCOM and the voltage drop across the linear reactor. The active and reactive powers of the system are depicted in Equations 49 and 50, where P is the active power, V_{bus} represents the bus terminal voltage, $V_{STATCOM}$ is the output voltage of the STATCOM, $X_L(=\omega L)$ is the inductive reactance, R is the resistance, ω is the angular frequency, L is the inductance, α is the phase angle between the bus and STATCOM voltages. The first term in Equation 50 is the reactive power demand due to the system, whilst the 2nd term is the reactive contribution by the STATCOM, where Q is the net reactive power that can be used to determine whether the STATCOM absorbs or injects reactive power [41].

$$P = \left(\frac{V_{bus} \times V_{STATCOM}}{X_L}\right) \times sin(\alpha) \quad (49)$$

$$Q = \left(V_{bus} \times \left(\frac{V_{bus}}{X_L}\right)\right) - \left(\frac{V_{bus} \times V_{STATCOM}}{X_L}\right) \times cos(\alpha) \quad (50)$$

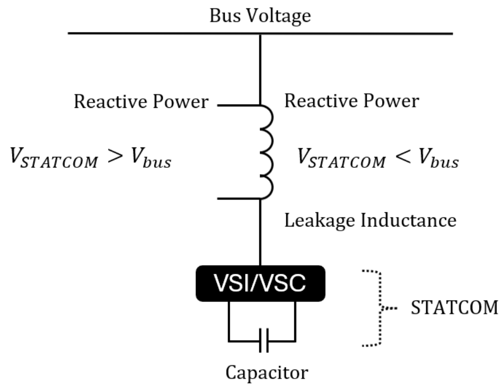

Fig. 21: Basic Operating Layout of a STATCOM

Source: created by the authors based on [41].

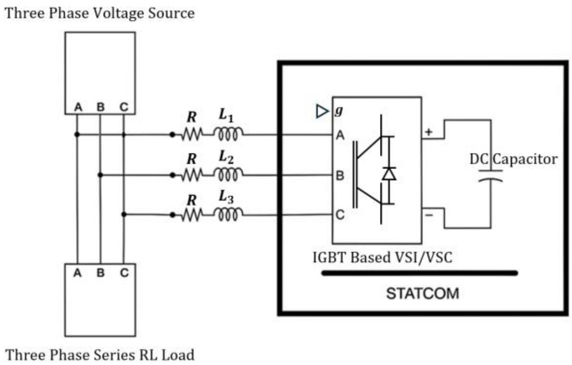

Fig. 22: Block Diagram of a STATCOM

Source: created by the authors based on [40], [41].

Using Figure 22, Equation 51 is derived from Kirchhoff's Voltage Law (KVL) applied to each phase of the STATCOM AC circuit, where x =phase a, b, c. Equation 52 is then derived by solving for $\frac{dI_{sx}}{dt}$, where E_{sx} represents the STATCOM internally generated voltage (for phase $\{a, b, c\}$), E_{tx} is the terminal voltage at the point of common coupling (PCC), I_{sx} is the STATCOM output current to the grid, R_s is the series resistance of the STATCOM, L_s is the series inductance and $\frac{dI_{sx}}{dt}$ is the rate of change of current. The Equations are then translated to a rotating reference frame, as depicted in Equation 53, where I_{sr} and I_{sl} are the STATCOM current components in the rotating reference frame, E_{sr} and E_{sl} are the STATCOM internal voltage components in the rotating reference frame, E_{tr} and E_{tl} are the terminal voltage components in the rotating reference frame and ω is the angular frequency, which simplifies the control as sinusoidal values will become DC values, which makes it easy to implement PI controllers for current or voltage regulation [41], [42].

$$E_{sx} - E_{tx} = R_s I_{sx} + L_s \left(\frac{dI_{sx}}{dt}\right) (51)$$
$$\frac{dI_{sx}}{dt} = \left(\frac{1}{L_s}\right) \times (-R_s \times I_{sx} + E_{sx} - E_{tx}) (52)$$
$$\begin{bmatrix} I_{sR} \\ I_{sl} \end{bmatrix} = \begin{bmatrix} \frac{-R_s}{L_s} & w0 \\ -w0 & \frac{-R_s}{L_s} \end{bmatrix} \begin{bmatrix} I_{sR} \\ I_{sl} \end{bmatrix} + \frac{1}{L_s} \begin{bmatrix} E_{sR} & E_{tR} \\ E_{sl} & E_{tl} \end{bmatrix} (53)$$

The DC-side voltage dynamics of the STATCOM are a critical part of the device, with the rate of change of the DC-link voltage represented by Equation 54, where V_{dc} represents the DC voltage across the DC capacitor of the STATCOM, $\frac{dV_{dc}}{dt}$ is the time derivative of the DC voltage, I_{dc} is the current flowing into the DC link from the AC side, C_s is the capacitance of the DC-link capacitor. The power conservation between the AC and DC sides is represented by Equation 55, which converts a two-axis system power expression to a three-phase system, where E_{sR} and E_{sI} represent the real and imaginary components of the AC-side inverter voltage and I_{sR} and I_{sI} are the real and imaginary components of the AC-side inverter current, respectively. Equations 56 and 57 express the output AC voltage vector of the STATCOM, where E_s is the magnitude of the AC-side inverter voltage vector, which is proportional to the DC link voltage and is scaled by the modulation constant K_{cs}, which is resolved on the real and imaginary axes using the modulation angle θs [41], [42].

Evaluated together, Equations 49 to 57 show that the STATCOM operates through direct regulation of converter voltage magnitude and phase relative to the point of common coupling. The essential analytical point is that reactive support is governed by the AC-side voltage differential, while the DC-link dynamics determine the energy balance needed to sustain converter action. In control terms, the dq-frame transformation converts sinusoidal AC variables into quasi-DC control variables, which allows the inner current loop and outer voltage loop to be coordinated with high bandwidth. This explains why STATCOM can respond substantially faster than mechanically or electromagnetically controlled alternatives and why its performance remains strong in weak grid and low-voltage operating conditions [38], [39], [40], [42].

$$\frac{dV_{dc}}{dt} = \left(\frac{1}{C_s}\right) \times (I_{dc}) (54)$$
$$V_{dc} \times I_{dc} = \left(\frac{3}{2}\right) \times (E_{sR} \times I_{sR} + E_{sI} \times I_{sI}) (55)$$
$$E_{sR} = E_s \times cos(\theta s) = K_{cs} \times V_{dc} \times cos(\theta s) (56)$$
$$E_{sI} = E_s \times sin(\theta s) = K_{cs} \times V_{dc} \times sin(\theta s) (57)$$

4 Synchronous Condensers

Synchronous Condensers provide instantaneous inertia to the grid and frequency response, and provide or absorb reactive power. In its over-excited state, it supplies reactive power. In its under-excited state, it absorbs reactive power. The key advantage of Synchronous Condensers over other devices is their wide-ranging controllability, which can result in reactive power generation from 50 percent lagging to full leading by adjusting their field current, which can be automatically paired with an effective integrated control system designed to maintain the power factor or voltage [42], [43].

Synchronous Condensers have numerous advantages and disadvantages [44], [45].

Advantages:

1. The power factor can be controlled because the current drawn by the Synchronous Condenser can be altered by changing the excitation field.
2. The ability to absorb and supply reactive power.
3. Sudden changes in the load can be adequately compensated for by the inertia of the Synchronous Condenser, which improves the system's stability.

Disadvantages:

1. High capital cost.
2. High maintenance.
3. Requires a startup mechanism.
4. Efficiency losses.
5. Limited dynamic response.

The basic structure and operation of Synchronous Condensers are similar to those of a Synchronous Machine in the absence of a prime mover, as shown in Figure 23. The Synchronous Condenser consists of a generator, excitation system, boost transformer system, starting system, cooling system, oil system, control system, and protection system. It absorbs minimal active power from the grid to maintain its loss [42], [45].

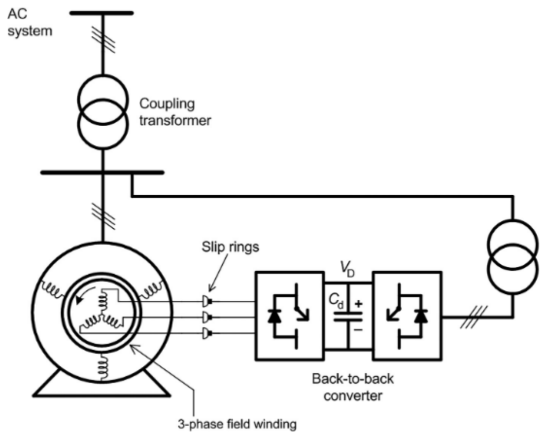

Fig. 23: Adjustable Speed Synchronous Condenser
Source: created by the authors based on [46].

In a synchronous machine, the stator houses the armature winding, whereas the rotor carries the field winding, as shown in Figure 24. Direct current is supplied to the rotor winding through carbon brushes that contact the slip rings that excite the rotor field. The DC source is termed the exciter and is typically mounted on the same shaft as a synchronous machine. The rotor pole surfaces were carefully shaped to ensure that the magnetic flux across the air gap varied in a smooth sinusoidal manner. This design helps the machine produce a clean sinusoidal voltage at its terminals, as depicted in Figure 25,where each revolution of the two poles indicates that the coil voltage goes through one complete cycle. It should be noted that the voltage frequency matches the rotor speed [44].

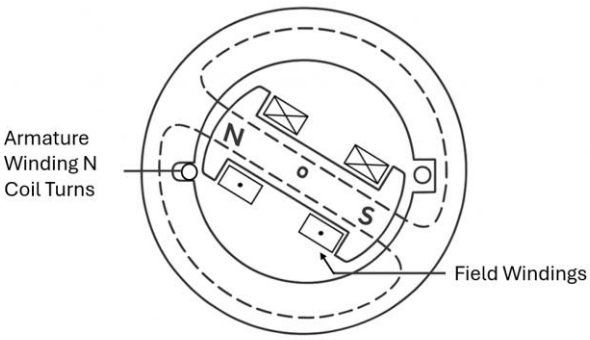

Fig. 24: Generic Sketch of a Synchronous Machine
Source: created by the authors based on [44].

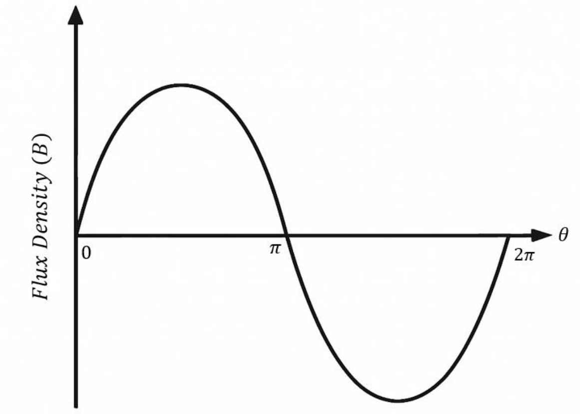

Fig. 25: Distribution of Flux Density in a Synchronous Generator
Source: created by the authors based on [44].

In a two-pole three-phase machine, the individual phase windings are 120 ° apart, as depicted in Figure 26 and illustrated in Figure 27. The magnetomotive forces owing to the current induced in the windings were also displaced by 120 °. The instantaneous values of the current for a balanced three-phase (phase sequence abc) operation are represented by Equation 58, where I_m is the maximum current value. The maximum current occurs when the instantaneous current in phase a reaches its positive peak. The Maximum magnetomotive force is depicted by Equation 59, where K is a constant that depends on the winding configuration (distribution per phase and turns), I_m is the maximum current value, i_a, i_b and i_c are the instantaneous phase currents, ω is the angular frequency, t is time and K is a constant that depends on the winding configuration (distribution per phase and turns). [18], [48].

$$\begin{cases} i_a = I_m \cos(\omega t) \\ i_b = I_m cos(\omega t - 120°) \\ i_c = I_m cos(\omega t - 240°) \end{cases} \quad (58)$$

$$F_{max} = \mathrm{K} I_m \quad (59)$$

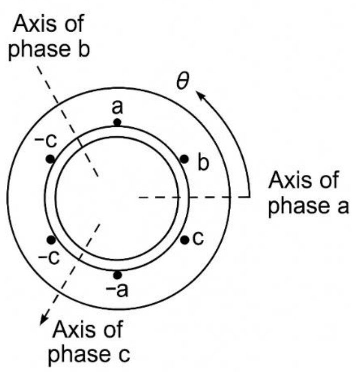

Fig. 26: Two-Pole, Three-Phase Stator Winding
Source: created by the authors based on [44].

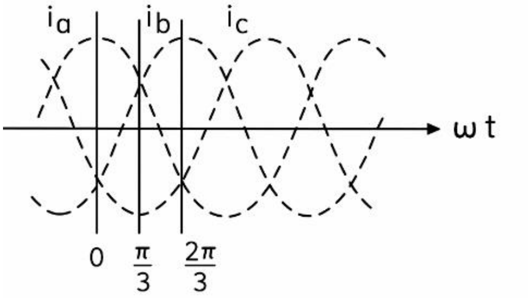

Fig. 27: Graphical Illustration of Three-Phase Currents

Source: created by the authors based on [44].

The MMF amplitude attributable to a particular phase component wave at a given instant $t$is represented by Equation 60, where $A_a(p)$, $A_b(p)$ and $A_c(p)$ are the amplitudes of the MMF components at point p for phases a, b and c, respectively, F_{max} is the maximum MMF amplitude, ω is the angular frequency and t is time [44], [47].

$$\begin{cases} A_{a(p)} = F_{\max} cos(\omega t) \\ A_{b(p)} = F_{\max} cos(\omega t - 120°) \\ A_{c(p)} = F_{\max} cos(\omega t - 240°) \end{cases} \quad (60)$$

The resultant MMF produced by the balanced three-phase currents at a spatial point p and electrical angle θ is given by Equation 61, where A_p is the resultant MMF, $A_a(p)$, $A_b(p)$ and $A_c(p)$ are the phase component MMFs at the point p and θ is the spatial angle. Equation 62 follows by substituting the phase MMF components from Equation 60. Using the trigonometric identity in Equation 63, the resultant MMF is simplified through Equations 64 and 65 [44], [47].

$$A_p = A_{a(p)} cos\theta + A_{b(p)} cos(\theta - 120) + A_{c(p)} cos(\theta - 240) \quad (61)$$

$$A_p = F_{\max}(cos\theta cos(\omega t) + cos(\theta - 120°) cos(\omega t - 120°) + cos(\theta - 240°) cos(\omega t - 240°)) \quad (62)$$

$$cos(\gamma) cos(\delta) = \left(\frac{1}{2}\right) [cos(\gamma - \delta) + cos(\gamma + \delta)] \quad (63)$$

$$A_p = \frac{1}{2} F_{\max}[\cos(\theta - \omega t) + \cos(\theta + \omega t) + \cos(\theta - \omega t) + \cos(\theta + \omega t - 240°) + \cos(\theta - \omega t) + \cos(\theta + \omega t - 480°)] \quad (64)$$

$$A_p = \left(\frac{3}{2}\right) F_{\max} cos(\theta - \omega t) \quad (65)$$

The MMF wave generated by the three-phase armature current is referred to as armature-reaction MMF. This wave rotates at a synchronous speed and is directly proportional to phase a when the current I_a reaches its maximum at t = 0. The DC field winding produces a sinusoidal MMF, denoted by F, whose axis leads to phase a by 90°, which is consistent with Faraday's law, as shown in Figure 28. The resultant magnetic field within the machine is the vector sum of the armature reaction and the field MMFs. As illustrated in Figure 28, the MMF of the field winding is shown by waveform F at the instant when the EMF in phase a owing to excitation is at its peak. This peak corresponds to the point where the rate of change of the flux linkage is the greatest; hence, the 90° lead. The armature-reaction MMF, which is shown as waveform A, is drawn in the opposite phase a because both I_a and the excitation EMF of the field E_f are at their maxima. The total magnetic field is represented by the resultant waveform R obtained by summing F and A [44], [47].

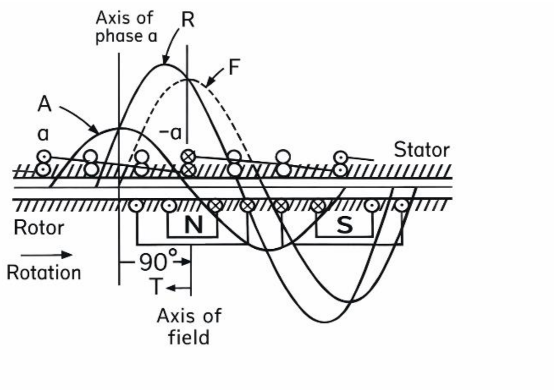

Fig. 28: Spatial MMF Waves in a Cylindrical Rotor Synchronous Generator

Source: created by the authors based on [44].

Waves A and F can be added using phasor notation. Figure 29 shows a phasor diagram representing the fluxes, whereϕ_f is the flux due to the field, ϕ_{ar} is the flux due to the armature current and ϕ_r is the resultant flux. Under the assumption of a uniform air gap and negligible magnetic saturation, the magnitudes of these fluxes are directly proportional to the respective MMF waveforms F, A, and R. Figure 30 represents the scenarioin which the armature current lags the excitation voltage, as represented by E_f [44], [47].

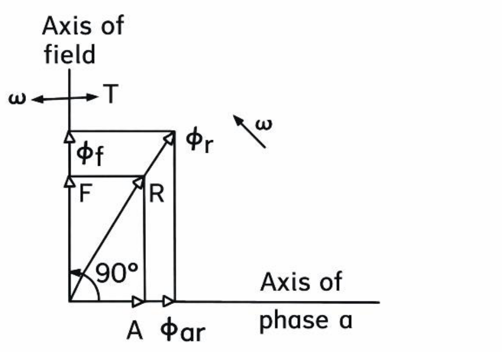

Fig. 29: A Space Phasor Diagram for Armature Current In Phase with Excitation Voltage
Source: created by the authors based on [44].

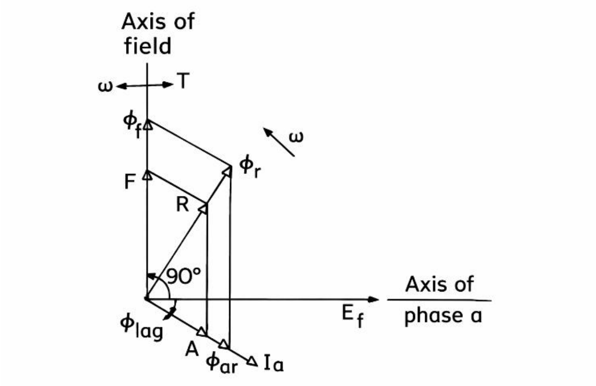

Fig. 30: A Space Phasor Diagram for Armature Current Lagging the Excitation Voltage
Source: created by the authors based on [44].

A simple equivalent circuit for a synchronous machine with a cylindrical rotor is essential for further analysis and interpretation. This can be obtained when the armature-reaction flux is modelled as an equivalent inductive reactance. This modelling approach is substantiated by the phasor diagram shown in Figure 31, which includes the component fluxes and corresponding voltages. The field flux, denoted as ϕ_f, was phasorially combined with the armature-reaction flux ϕ_{ar} to produce the resultant air-gap flux ϕ_{r}. The armature reaction flux and armature current were in phase. The excitation voltage E_f is induced by the field flux ϕ_f where the excitation voltage lags the field flux by 90 °in accordance with Faraday's law of electromagnetic induction. The voltages for the armature reaction E_{ar} and the resultant internal air gap E_{r} also lag the flux by 90 °. The armature reaction voltage is represented by Equation 66, where x_Φ represents the constant of proportionality (correlates to the rms values of E_{ar} & I_a), I_a is the stator current and j is the imaginary unit, with $-j$ indicating a 90° phase shift (lagging). Similarly, the resultant airgap voltage is given by Equations 67 [44] and [47].

$E_{ar} = -jx_\Phi I_a$(66)
$E_r = E_f - jx_\Phi I_a$(67)

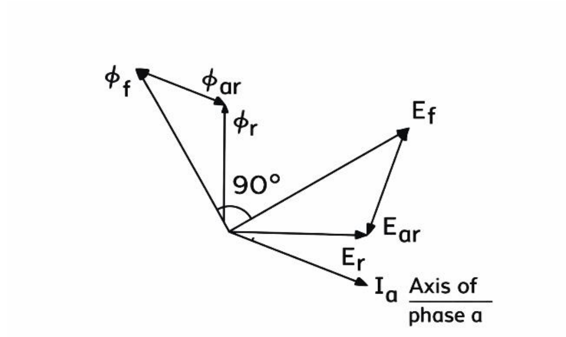

Fig. 31: Phasor Diagram Representing the Fluxes and Resulting Voltages in A Synchronous Machine
Source: created by the authors based on [44].

Equation 67 can be used to produce an equivalent circuit, as depicted in Figure 32, and it follows that the inductive reactance x_ϕ accounts for the impact of the armature reaction effects. This is known as the magnetizing reactance of the machine, and the terminal voltage of the machine V_t, which is obtained by determining the difference between the air-gap voltage and the voltage drop, which is due to the armature resistance r_a and the leakage reactance x_l. The reactance x_l represents the combined effects of the leakage flux and space harmonic fields that are not captured by the magnetizing reactance x_ϕ. A composite impedance, referred to as the synchronous impedance Z_s, is represented by Equation 68, where X_s represents the synchronous reactance, j is the imaginary unit, E_f is the excitation voltage and I_a is the armature current, which is represented by Equation 69. The excitation voltage for an unsaturated cylindrical rotor synchronous machine operating under balanced polyphase load conditions is given by Equation 70 [44], [48].

$Z_s = r_a + jX_s$(68)
$X_s = x_l + x_\Phi$(69)
$E_f = V_t + I_a Z_s$(70)

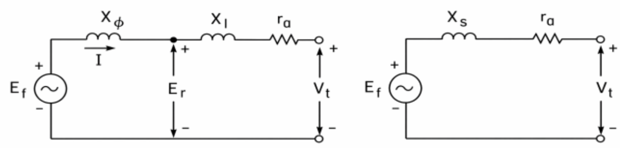

Fig. 32: Two Equivalent Circuits for the Synchronous Machine
Source: created by the authors based on [44].

The main objective of the synchronous impedance method is to determine the synchronous reactance X_s by performing both open-circuit and short-circuit tests [48].

1. In the open-circuit test, the generator was operated at its rated speed with the terminals open. The field current

I_f is varied, the corresponding terminal voltage, V_{oc} is recorded. As no current flows in the armature, there is no voltage drop across the internal impedance, resulting in an open-circuit voltage equating to the internally generated EMF, as shown in Equation 71.

$$E_f = V_{oc} \quad (71)$$

2. In the short-circuit test, the generator terminals were short-circuited using ammeters, where the field current varied and the corresponding armature current I_{asc} was recorded. The terminal voltage is zero under this specific condition, and an internally generated voltage E_f appears across the synchronous impedance Z_s, as shown in Equation 72, where E_f is the internally generated voltage and Z_s is the synchronous impedance.

$$Z_s = \frac{E_f}{I_{asc}} \quad (72)$$

3. The synchronous impedance Z_s consists of the armature resistance R_a and synchronous reactance X_s and is represented by Equation 73, where j is the imaginary unit. When R_a is known, Equation 74 applies, and when R_a is negligible, Equation 75 applies, where E_f is the internally generated voltage and I_{asc} is the short-circuit armature current.

$$Z_s = R_a + jX_s \quad (73)$$
$$X_s = \sqrt{Z_s^2 - R_a^2} \quad (74)$$
$$X_s \approx \frac{E_f}{I_{asc}} \quad (75)$$

This method has a wide array of uses, which include:

1. The prediction of voltage regulation of synchronous generators under varying loading conditions.
2. The estimation of the internal parameters of the machine, such as synchronous reactance, is required for power system modelling.
3. Allows for an approximate Fault Analysis and determination of short-circuit current levels.

To illustrate the power angle characteristic using the infinite bus approximation, the simplified network of Figure 34 is considered with reference to Figure 33, where E is the sending-end voltage, V is the receiving-end voltage, Z is the transfer impedance and δ is the angle between E and V, which governs the magnitude and direction of power transfer, as depicted in Equations 76 to 78. The corresponding current is given by Equation 79 in phasor form based on Ohm's law and is further expanded in Equation 80, where I is the current and ψ is the phase angle [44], [49].

$$E = E \angle\delta \quad (76)$$
$$V = V \angle 0 \quad (77)$$
$$Z = Z \angle\psi \quad (78)$$
$$I = \frac{E-V}{Z} \quad (79)$$
$$I = \frac{E}{Z}\angle(\delta - \psi) - \frac{V}{Z}\angle(-\psi) \quad (80)$$

The phasor-domain Equations below and above correlate with the power flow in a transmission line, which is vital in power flow studies, transient stability, and economic dispatch in power systems. Equations 81 to 84 represent the complex power at both the sending and receiving ends in simplified and expanded phasor equations, where S_1^* represents the complex power at the sending end, S_2^* represents the complex power at the receiving end and $(.)^*$ denotes the complex conjugate [44], [49].

$$S_1^* = E \cdot I \quad (81)$$
$$S_2^* = V \cdot I \quad (82)$$
$$S_1^* = \frac{E^2}{Z}\angle(-\psi) - \frac{EV}{Z}\angle(-\psi - \delta) \quad (83)$$
$$S_2^* = \frac{EV}{Z}\angle(\delta - \psi) - \frac{V^2}{Z}\angle(-\psi) \quad (84)$$

Equations 85 to 88 are derived using phasor algebra and complex power expressions in transmission lines, which represent the active and reactive powers for both the sending and receiving ends, where P_1 and Q_1 are the sending-end active and reactive powers, respectively, P_2 and Q_2 are the receiving-end active and reactive powers, respectively, E is the sending-end voltage magnitude, V is the receiving end voltage magnitude and Z is the transfer impedance magnitude. They show that both the sending and receiving end powers depend on the impedance angle ψ, which accounts for line resistance and reactance; if $\psi = 90°$And the line is purely reactive; the equations are further simplified. The power angle δ represents the extent to which the sending and receiving voltages are out of phase and is one of the key factors in real power flow. The active and reactive power equations are further reduced in Equations 89 to 91, where X is the transfer reactance of the purely reactive line [44], [49].

$$P_1 = \frac{E^2}{Z}\cos(-\psi) - \frac{EV}{Z}\cos(\psi + \delta) (85)$$
$$Q_1 = \frac{E^2}{Z}\sin(\psi) - \frac{EV}{Z}\sin(\psi + \delta) (86)$$
$$P_2 = \frac{EV}{Z}\cos(\delta - \psi) - \frac{V^2}{Z}\cos(\psi) (87)$$
$$Q_2 = \frac{EV}{Z}\sin(\psi - \delta) - \frac{V^2}{Z}\sin(\psi) (88)$$
$$P_1 = P_2 = \frac{EV}{X}\sin(\delta) (89)$$
$$Q_1 = \frac{E^2 - EV\cos(\delta)}{X} (90)$$
$$Q_2 = \frac{EV\cos(\delta) - V^2}{X} (91)$$

In large-scale power networks, a three-phase synchronous generator is typically connected to a grid through an equivalent reactance. This setup is particularly common when the grid's overall generating capacity far exceeds that of any single unit. In such cases, the grid is often treated as an infinite bus, as depicted in Figure 34, meaning that its voltage and frequency remain effectively constant regardless of the changes made by a single generator. Consequently, when a generator is tied to this type of system, its operating conditions, including terminal voltage and system frequency, are controlled by the grid itself and not by the generator's internal dynamics. Equation 92 is the power transfer equation, where P is the transferred active power and δ is the power angle between the generator internal EMF E and the infinite-bus voltage V, which describes how the power transfer varies with δ. Equation 93 depicts the maximum power transfer, where P_{max} is the maximum power transfer, which predicts that the greater the internal excitation E or infinite-bus voltage V, the more power can be transferred, where X_t represents the total transfer reactance between the generator and the system, which is more commonly known as the steady-state stability limit. Equation 94 combines the reactance of the generator and the network to summarize the total opposition to power flow, where X_s is the generator synchronous reactance and X_e is the equivalent reactance of the transmission network between the generator and the infinite bus [18], [44], [49].

$$P = P_{max}\sin\delta (92)$$
$$P_{max} = \frac{EV}{X_t} (93)$$

$$X_t = X_s + X_e (94)$$

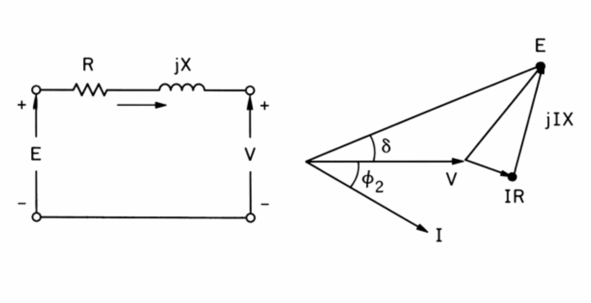

Fig. 33: Equivalent circuit and Phasor Diagram
Source: created by the authors based on [44].

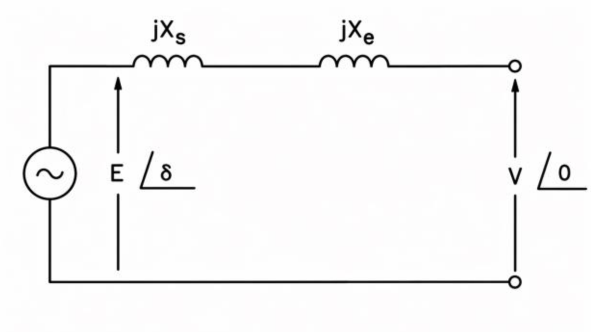

Fig. 34: Synchronous Machine Connected to an Infinite Bus
Source: created by the authors based on [44].

A synchronous generator can either produce or absorb reactive power based on the relationship among its internal EMF, power angle δ and terminal voltage V. The generator produces reactive power when Q_2 is greater than 0; in this state, the machine is over-excited and behaves like a capacitor in the system and meets the condition as per Equation 95. The generator can also absorb reactive power when Q_2 is less than 0; in this state, the machine is excited, behaves like an inductor, and meets the condition as per Equation 96. The machine can also operate with a zero-power angle, which is typical when the machine functions as a Synchronous Condenser with the reactive power simplified as per Equation 97 [44], [49].

Equations 95 to 97 clarify the reactive-power operating conditions of the Synchronous Condenser, where E is the generator's internal EMF, V is the terminal or infinite-bus voltage, δ is the power angle, Q_2 is the reactive power and X is the transfer. reactance between the machine and the system. The machine produces reactive power when $E\cos\delta > V$, absorbs reactive power when $E\cos\delta < V$ and under near-zero active-power operation, the reactive power is given by Equation 97. The Synchronous Condenser influences the network through the internal EMF power-angle relationship of a rotating synchronous machine, so changes in excitation affect not only reactive-power output but also synchronizing torque, short-circuit contribution and electromechanical resilience. When operated close to zero active-power exchange, the machine behaves as a controllable reactive source whose voltage-support capability is backed by physical inertia and electromagnetic fault-current strength. This combination is the principal reason why Synchronous Condensers continue to be selected where short-circuit ratio, post-fault voltage recovery, and overall grid strength are limiting factors [18], [42], [44], [49].

$$E \cos \delta > V \quad (95)$$
$$E \cos \delta < V \quad (96)$$
$$Q_2 = \frac{V(E-V)}{X} \quad (97)$$

5 Plant Size

Synchronous Condensers are relatively large devices, with typical plant sizes measuring thousands of square meters, and the cost per kVar produced varies in relation to various factors, including design complexity, size, manufacturing processes, and cooling systems. These robust devices also experience high maintenance costs and internal losses; however, they provide a reliable source of reactive power, which significantly improves grid stability and is easily accessed by the system operator and needs to be quantified from a financial perspective [51].

FACTS devices have a smaller footprint than a Synchronous Condenser with similar reactive power outputs and lower maintenance costs; however, they do not provide all the benefits of a Synchronous Condenser, including the inertial response of the rotating parts and a reduced availability factor, in addition to having a lower short-circuit contribution [52], [53].

6 Unified Stability Metrics for Comparative Assessment

For comparative assessment, the technologies reviewed in this paper can be mapped to a common set of stability-oriented metrics. For voltage stability, the most direct screening quantity is the local voltage sensitivity to reactive power, expressed in small signal form as $S_{VQ} = \partial V / \partial Q$. A smaller magnitude of S_{VQ}, or equivalently a larger inverse sensitivity $|\partial Q/\partial V|$, indicates a stronger voltage support condition. This metric may be complemented by voltage collapse proximity indicators, reactive-power margin, and maximum-loadability measures to quantify how close the operating point is to the collapse boundary [55], [56], [57].

For transient stability, the principal system-level indicators are the critical clearing time (CCT), the maximum rotor-angle deviation $\Delta\delta_{max}$ and, where relevant, the transient energy margin. Devices that improve post-fault voltage support or synchronizing torque tend to increase CCT and reduce $\Delta\delta_{max}$. In this sense, series compensation chiefly influences transient power transfer through the transfer reactance, while shunt devices and Synchronous Condensers primarily support transient recovery through voltage restoration and reactive-current or excitation response [18], [58], [59].

For oscillatory stability, a standard small-signal metric is the damping ratio of the i-th oscillatory mode, given by:

$$\zeta_i = \frac{-\sigma_i}{\sqrt{(\sigma_i^2 + \omega_i^2)}} \quad (98)$$

where σ_i and ω_i are the real and imaginary parts of the i-th eigenvalue $\lambda_i = \sigma_i \pm j\omega_i$. The associated participation factor, $p_{ki} = \varphi_{ki}\, \psi_{ik}$, identifies the states that dominate that mode and helps determine whether damping improvement should be obtained through voltage control, impedance modulation, or excitation control [60]. Taken together, S_{VQ}, voltage collapse proximity, CCT, $\Delta\delta_{\max}$ and ζ_i provide a consistent comparative basis for comparing shunt FACTS devices, series FACTS devices, Synchronous Condensers under high-PV operating conditions [18], [55], [56], [57], [58], [59], [60].

Table 2. Comparative classification and operational properties of the reviewed technologies
Source: compiled by the authors based on [18], [24], [25], [34], [35], [39], [42], [45], [52].

Feature	TCSC	TSSC	SVC	STATCOM	Synchronous Condenser
Basic type (grid connection)	Series, thyristor-controlled.	Series, thyristor-switched (stepwise).	Shunt, thyristor-controlled reactors/capacitors.	Shunt, voltage-source-converter-based.	Shunt, rotating synchronous machine.
Primary control channel	Variable series reactance.	Discrete series capacitive insertion.	Variable shunt reactive power.	Fast continuous shunt reactive power.	Excitation-controlled reactive power

					with inertia.
Control mechanism	Firing-angle control of the thyristor-controlled reactor.	Switching of capacitor segments at discrete steps.	Coordinated TCR/TSC control.	Converter voltage magnitude and phase control.	Field-excitation control of a synchronous machine.
Response time	Fast; typically, less than one cycle.	Fast but stepwise; slower than TCSC.	Fast; typically, 1–2 cycles.	Very fast; sub-cycle response possible.	Slower; governed by electromechanical time constants.
Voltage support	Indirect, through line-reactance control.	Indirect, through stepwise series compensation.	Direct shunt voltage support.	Direct shunt voltage support with strong dynamic behaviour.	Strong voltage support through excitation control.
Power flow control	Moderate to high.	Moderate; stepwise.	Indirect.	Indirect through voltage control, but highly dynamic.	Indirect through voltage regulation and VAR support.
Harmonic behaviour	Moderate harmonic distortion possible.	Moderate harmonic distortion possible.	Higher harmonic concern due to thyristor operation.	Low to moderate, depending on converter design and filtering.	Negligible converter-related harmonics.
Short-circuit contribution	Low.	Low.	Low.	Medium relative to other electronic devices, but still limited compared with rotating machines.	High.
Inertia contribution	None.	None.	None.	None.	Yes.
Support in weak grids	Limited.	Limited.	Moderate.	Highly effective.	Highly effective.
Support during faults	Susceptible to commutation-related limitations.	Typically bypassed during severe faults.	Voltage support available but with limited fault contribution.	Strong dynamic voltage support and ride-through assistance.	Sustained support if excitation is maintained.
Installation location	In series with transmission lines.	In series with transmission lines.	At substation busbars.	At substation busbars.	Substations or near load/generation centers.
Maintenance level	Moderate.	Low to moderate.	Moderate.	Low to moderate.	High.
Typical applications	Power flow control, SSR mitigation, damping.	Cost-effective discrete series compensation.	Voltage support and stability enhancement.	Fast voltage regulation and weak grid support.	Inertia provision, voltage regulation and fault-level support.

Table 2. consolidates the comparative characteristics of the reviewed technologies and shows that they separate naturally into three control classes. Series controllers (TCSC, TSSC, and SSSC) primarily influence effective line reactance and are therefore strongest in power flow shaping and oscillation-related applications. Shunt electronic devices (SVC and STATCOM) act directly on bus voltage through controllable reactive-power injection, with the STATCOM providing the fastest dynamic response and the strongest low-voltage reactive behaviour. The Synchronous Condenser is slower but uniquely combines steady reactive support with inertia and substantial short-circuit contribution, which explains its continuing importance in weak grid renewable integration [18], [24], [25], [34], [35], [39], [42], [45], [52]

The response time, harmonic behaviour and short-circuit contribution statements in Table 2 should be interpreted together with the device-specific discussions in Sections 3.2 to 3.6 and the synchronous-machine analysis in Section 4 for completeness.

7 Conclusions & Outlook

This review has shown that FACTS devices and Synchronous Condensers address high-PV stability challenges through fundamentally different control mechanisms and should therefore be evaluated against the dominant system limitation rather than through a single generic ranking. Series-FACTS devices principally modify transfer reactance and are strongest in power flow control, congestion relief, and oscillation damping. Shunt electronic compensators primarily provide fast reactive-power support and voltage regulation, with the STATCOM offering the strongest dynamic performance under weak grid or depressed voltage conditions. Synchronous Condensers provide slower control action, but uniquely contribute inertia, short-circuit strength and robust post-fault voltage support [17], [18], [25], [34], [39], [42], [44].

It is evident that neither technology can be considered superior to the other, as each exhibits its own coherent strengths and limitations that align with specific grid applications and power system requirements. In general, FACTS controllers excel in rapid control and modular scalability, whereas Synchronous Condensers provide system strength and resilience in weak networks with high levels of renewable energy penetration. This comparative analysis highlights that future power systems will require coordinated deployment of both technologies in response to specific system requirements.

Although both FACTS devices and Synchronous Condensers have been applied to similar classes of power system instability, they are not often evaluated within a single unified framework tailored to high-PV operating conditions. Their performance should therefore be assessed against a consistent set of criteria, including reactive-power controllability, dynamic voltage support, response speed, oscillation damping capability, short-circuit contribution, inertial support, and system losses [50].

Several metrics can be developed to measure the degree of power system stability and facilitate quantification of the level of system resilience and vulnerability under varying operational scenarios. This can be accomplished by utilizing the principal dimensions of power system stability addressed in this review, namely voltage stability, transient stability, and oscillatory stability [54], [55].

These metrics capture the performance of reactive-power support technologies in terms of reactive-power controllability, dynamic voltage support during disturbances, transient response, oscillation damping capability, contribution to short-circuit strength, inertial support and influence on overall system losses.

The principal value of the present paper lies in the use of a common evaluation framework that assesses reactive-power controllability, dynamic response, voltage-support capability, oscillatory behaviour, short-circuit contribution and implementation burden across technologies that are frequently discussed in separate literature streams. Under this framework, no single device is universally optimal. The technically appropriate choice depends on whether the governing constraint is transfer capability, voltage weakness, low fault level, oscillatory behaviour, or the need for combined electrical and electromechanical strength.

Accordingly, future planning in high-PV networks is likely to rely on coordinated deployment rather than a single technology selection. Converter-based compensation is well matched to fast voltage control and modular reinforcement, whereas Synchronous Condensers remain particularly valuable where grid strength, inertia and fault-current support must be restored. A rigorous next step is to apply the explicit stability metrics introduced in this review within utility-specific studies so that technical performance and economic screening can be assessed on a consistent basis.

A further extension of this review is the use of simplified benchmark test systems and sensitivity studies to quantify how variations in grid strength, fault level, and reactive-power demand influence the comparative performance of series FACTS devices, shunt FACTS devices, and Synchronous Condensers under high-PV operating conditions.

Acknowledgment
The authors gratefully acknowledge the support and encouragement received from family, colleagues, and the Discipline of Electrical, Electronic and Computer Engineering at the University of KwaZulu-Natal during the preparation of this manuscript.

References:

[1] GreenCape, Large-Scale Renewable Energy: Market Intelligence Report (MIR) 2023, 2023. Accessed: Feb. 5, 2025. [Online]. Available: https://greencape.co.za/wpcontent/uploads/2023/04/RENEWABLE_ENERGY_MIR_2023_DIGITAL_SINGLES.pdf

[2] C. J. H. Hartnady, "South Africa's diminishing coal reserves," South Afr. J. Sci., vol. 106, no. 9/10, p. 5 pages, Sep. 2010, doi: 10.4102/sajs.v106i9/10.369.

[3] Intergovernmental Panel on Climate Change (IPCC), Climate Change 2023: Synthesis Report. Contribution of Working Groups I, II and III to the Sixth Assessment Report of the Intergovernmental Panel on Climate Change, H. Lee and J. Romero, Eds. Geneva, Switzerland: IPCC, 2023. doi: 10.59327/IPCC/AR6-9789291691647.

[4] M. Perez and R. Perez, "Update 2022 – A fundamental look at supply side energy reserves for the planet," Sol. Energy Adv., vol. 2, p. 100014, 2022, doi: 10.1016/j.seja.2022.100014.
[5] Solar Energy Industries Association (SEIA), "US Solar Market Insight: 2024 Year in Review – Executive Summary," 2025. Accessed: Feb. 10,2025.[Online].Available: .https://seia.org/wpcontent/uploads/2025/03/SMI-2024-YIR-ES.pdf.
[6] Council for Scientific and Industrial Research (CSIR), "Utility Statistics Report: Jan 2025 (Final)," 2025. Accessed: Feb. 20, 2025. [Online].Available: https://www.csir.co.za/sites/default/files/202509/Utility%20Statistics%20Report_Jan%202025_Final.pdf.
[7] G. C. Mahato, T. R. Choudhury and B. Nayak, "A Review on High PV Penetration on Smart Grid: Challenges and its Mitigation using FPPT," in Proc. 2021 1st International Conference on Power Electronics and Energy (ICPEE), Bhubaneswar, India, 2021, pp. 1–6, doi: 10.1109/ICPEE50452.2021.9358474.
[8] A. Hansa, C. Ndlhovu, M. Theku and J. Machinjike, "Synchronous Condenser Optimisation Study – Strategic Grid Planning," unpublished internal report, Eskom Holdings SOC Ltd., South Africa, n.d.
[9] M. Karimi, H. Mokhlis, K. Naidu, S. Uddin and A. H. A. Bakar, "Photovoltaic penetration issues and impacts in distribution network – A review," Renew. Sustain. Energy Rev., vol. 53, pp. 594–605, Jan. 2016, doi: 10.1016/j.rser.2015.08.042.
[10] J. Wong, Y. S. Lim, J. H. Tang and E. Morris, "Grid-connected photovoltaic system in Malaysia: A review on voltage issues," Renew. Sustain. Energy Rev., vol. 29, pp. 535–545, Jan. 2014, doi: 10.1016/j.rser.2013.08.087.
[11] J. L. M. Pereira, A. F. R. Leal, G. O. D. Almeida and M. E. D. L. Tostes, "Harmonic Effects Due to the High Penetration of Photovoltaic Generation into a Distribution System," Energies, vol. 14, no. 13, p. 4021, Jul. 2021, doi: 10.3390/en14134021.
[12] S. Bhattacharya, T. Saha and M. J. Hossain, "Fault current contribution from photovoltaic systems in residential power networks," in 2013 Australasian Universities Power Engineering Conference (AUPEC), Hobart, Australia: IEEE, Sep. 2013, pp. 1–6. doi: 10.1109/AUPEC.2013.6725450.
[13] I. Kim, "A calculation method for the short-circuit current contribution of current-control inverter-based distributed generation sources at balanced conditions," Electr. Power Syst. Res., vol. 190, p. 106839, Jan. 2021, doi: 10.1016/j.epsr.2020.106839.
[14] J. D. Glover, M. S. Sarma and T. J. Overbye, Power System Analysis and Design, 4th ed. Stamford, CT, USA: Thomson, 2008, p. 255.
[15] A. R. Bergen and V. Vittal, Power Systems Analysis, 2nd ed. Upper Saddle River, NJ, USA: Prentice Hall, 2000.
[16] F. Katiraei and J. Aguero, "Solar PV Integration Challenges," IEEE Power Energy Mag., vol. 9, no. 3, pp. 62–71, May 2011, doi: 10.1109/MPE.2011.940579.
[17] K. R. Padiyar, FACTS Controllers in Power Transmission and Distribution. New Delhi, India: New Age Int. Publishers, 2007.
[18] P. Kundur, Power System Stability and Control. New York, NY, USA: McGraw-Hill, 1994.
[19] S. H. Khader and A. K. K. Daud, "Single-phase AC supply," in Electric Renewable Energy Systems, Elsevier, 2016, pp. 156–182. doi: 10.1016/B978-0-12-804448-3.00009-8.
[20] B. Fani, M. Mahdavian and S. Javadi, "Shunt FACTS controller: Classification, modeling, operation and control techniques," in 2017 14th International Conference on Electrical Engineering/Electronics, Computer, Telecommunications and Information Technology (ECTI-CON), Phuket: IEEE, Jun. 2017, pp. 50–53. doi: 10.1109/ECTICon.2017.8096170.
[21] D. I. I. Alabi, D. A. I. Araga and A. O. Anibasa, "Design of Power Oscillation Damper for UPFC Controllers Embeded in the Nigerian National Grid," American Journal of Engineering Research (AJER), vol. 6, no. 1, pp. 107–116, 2017.
[22] G. Shahgholian, M. Mahdavian, M. Janghorbani, I. Eshaghpour and E. Ganji, "Analysis and simulation of UPFC in electrical power system for power flow control," in 2017 14th International Conference on Electrical Engineering/Electronics, Computer, Telecommunications and Information Technology (ECTI-CON), Phuket: IEEE, Jun. 2017, pp. 62–65. doi: 10.1109/ECTICon.2017.8096173.
[23] A. Gavrilović, W. Williams, H. Thanawala and D. Young, "Reactive Power Plant and

FACTS Controllers," in Electrical Engineer's Reference Book. Oxford, U.K.: Elsevier, 2003, pp. 41-1–41-40. doi: 10.1016/B978-075064637-6/50041-1.

[24] IEEE Std 1534-2009, IEEE Recommended Practice for Specifying Thyristor-Controlled Series Capacitors. New York, NY, USA: IEEE, 2009.

[25] N. G. Hingorani and L. Gyugyi, Understanding FACTS: Concepts and Technology of Flexible AC Transmission Systems. New York, NY, USA: IEEE Press, 2000. doi: 10.1109/9780470546802.

[26] D. Kalpaktsoglou, A. Tsiakalos, S. Pouros and M. Roumeliotis, "Comparison between Thyristor Switched Series Capacitors and Thyristor Switched Parallel Capacitors for wind power systems - A Simulation Study," WSEAS Trans. POWER Syst., vol. 15, pp. 257–264, Jan. 2021, doi: 10.37394/232016.2020.15.30.

[27] R. Mihali, "Static synchronous series compensator—a means for dynamic power flow control in electric power systems," WSEAS Transactions on Power Systems, vol. 1, no. 1, pp. 90–97, Jan. 2006.

[28] E. H. Sadiq, L. A. Mohammed and H. M. Taha, "Enhancing Power Transmission Efficiency Using Static Synchronous Series Compensators: A Comprehensive Review," J. Intell. Syst. Control, vol. 3, no. 2, pp. 71–83, Jun. 2024, doi: 10.56578/jisc030201.

[29] N. G. Hingorani, "Static synchronous series compensator: A solid-state approach to the series compensation of transmission lines," IEEE Power Engineering Review, vol. 9, no. 5, pp. 22–23, May 1989. doi: 10.1109/MPER.1989.4310794.

[30] K. K. Sen, "SSSC-static synchronous series compensator: theory, modeling and application," IEEE Trans. Power Deliv., vol. 13, no. 1, pp. 241–246, Jan. 1998, doi: 10.1109/61.660884.

[31] S. V. Smolovik, V. S. Chudny, A. I. Denisenko, A. S. Liamov and A. L. Tupitsina, "Control Characteristics of Static Synchronous Series Compensator," in 2020 IEEE Conference of Russian Young Researchers in Electrical and Electronic Engineering (EIConRus), St. Petersburg and Moscow, Russia: IEEE, Jan. 2020, pp. 1329–1332. doi: 10.1109/EIConRus49466.2020.9039313.

[32] S. K. Gupta, "FACTS and Its Application," presented at the One Day Seminar on Recent Developments in Flexible AC Transmission System, Northern India Engineering College, New Delhi, India, Oct. 2007.

[33] S. K. Srivastava, S. N. Singh and K. G. Upadhyay, "FACTS devices and their controllers: An overview," in Proc. National Power Systems Conference (NPSC), IIT Kharagpur, India, Dec. 2002, pp. 651–657.

[34] M. Eremia, A. Gole and L. Toma, "Static VAR Compensator (SVC)," in Advanced Solutions in Power Systems: HVDC, FACTS and Artificial Intelligence, 1st ed., M. Eremia, C. Liu and A. Edris, Eds. Hoboken, NJ, USA: Wiley, 2016, pp. 271–338. doi: 10.1002/9781119175391.ch5.

[35] R. M. Mathur and R. K. Varma, Thyristor-Based FACTS Controllers for Electrical Transmission Systems. IEEE, 2002. doi: 10.1109/9780470546680.

[36] N. Mohan, T. M. Undeland and W. P. Robbins, Power Electronics: Converters, Applications and Design, 2nd ed. New York, NY, USA: Wiley, 1995.

[37] IEEE Recommended Practice and Requirements for Harmonic Control in Electric Power Systems. New York, NY, USA: IEEE, 2014. doi: 10.1109/IEEESTD.2014.6826459.

[38] Zhengping Xi and S. Bhattacharya, "STATCOM Control and Operation with Series Connected Transformer Based 48-pulse VSC," in IECON 2007 - 33rd Annual Conference of the IEEE Industrial Electronics Society, Taipei: IEEE, Nov. 2007, pp. 1714–1719. doi: 10.1109/IECON.2007.4460359.

[39] IEEE Std 1031-2011, IEEE Guide for the Functional Specification of Transmission Static Var Compensators. Piscataway, NJ, USA: IEEE, 2011, doi: 10.1109/IEEESTD.2011.5936078.

[40] P. S. Borse, D. A. G. Thosar and S. Shaha, "Modeling and simulation of STATCOM," International Journal of Engineering Research (IJER), vol. 3, no. 12, pp. 705–708, Dec. 2014.

[41] K. V. Patil, "Dynamic Compensation of Electrical Power Systems Using a New BVSI STATCOM," Ph.D. dissertation, Dept. Electr. Comput. Eng., Univ. Western Ontario, London, ON, Canada, 1999.

[42] Y. Liu et al., "Review on Synchronous Condenser Modeling Study," in 2018 China International Conference on Electricity Distribution, Tianjin, China, 2018, pp. 227–232, doi: 10.1109/CICED.2018.8592360.

[43] M. E. El-Hawary, Electrical Power Systems: Design and Analysis, rev. printing. New York, NY, USA: IEEE Press/Wiley-Interscience, 1995. doi: 10.1109/9780470544464.

[44] B. M. Weedy, B. J. Cory, N. Jenkins, J. B. Ekanayake and G. Strbac, Electric Power Systems, 5th ed. Hoboken, NJ, USA: Wiley, 2012.

[45] E. H. Watanabe, F. K. De A. Lima, R. F. Da Silva Dias, M. Aredes, P. G. Barbosa and S. L. S. Lima Barcelos, "Flexible AC Transmission Systems," in Power Electronics Handbook, Elsevier, 2024, pp. 909–937. doi: 10.1016/B978-0-323-99216-9.00038-X.

[46] A. E. Fitzgerald, C. Kingsley and S. D. Umans, Electric Machinery, 6th ed., Int. ed. Boston, MA, USA: McGraw-Hill, 2009.

[47] S. J. Chapman, Electric Machinery Fundamentals, 5th ed. New York, NY, USA: McGraw-Hill, 2012.

[48] J. J. Grainger and W. D. Stevenson, Power System Analysis. New York, NY, USA: McGraw-Hill, 1994.

[49] A. Nikolaou, Y. Guo, E. Batzelis and B. C. Pal, "Dynamic Voltage Support of Grid-Forming Inverters," May 13, 2024, Preprints. doi: 10.36227/techrxiv.171560731.10711174/v1.

[50] F. O. Igbinovia, G. Fandi, Z. Muller, J. Svec and J. Tlusty, "Cost implication and reactive power generating potential of the Synchronous Condenser," in 2016 2nd International Conference on Intelligent Green Building and Smart Grid (IGBSG), Prague, Czech Republic: IEEE, Jun. 2016, pp. 1–6. doi: 10.1109/IGBSG.2016.7539450.

[51] A. Siddique, Y. Xu, W. Aslam and M. Rasheed, "A Comprehensive Study on FACTS Devices to Improve the Stability and Power Flow Capability in Power System," in 2019 IEEE Asia Power and Energy Engineering Conference (APEEC), Chengdu, China: IEEE, Mar. 2019, pp. 199–205. doi: 10.1109/APEEC.2019.8720685.

[52] N. Nimpitiwan, G. T. Heydt, R. Ayyanar and S. Suryanarayanan, "Fault Current Contribution From Synchronous Machine and Inverter Based Distributed Generators," IEEE Trans. Power Deliv., vol. 22, no. 1, pp. 634–641, Jan. 2007, doi: 10.1109/TPWRD.2006.881440.

[53] K. Eshghi, B. K. Johnson and C. G. Rieger, "Metrics required for power system resilient operations and protection," in 2016 Resilience Week (RWS), Chicago, IL, USA: IEEE, Aug. 2016, pp. 200–203. doi: 10.1109/RWEEK.2016.7573333.

[54] M. Nedd, W. Bukhsh, C. MacIver and K. Bell, "Metrics for determining the frequency stability limits of a power system: A GB case study," Electr. Power Syst. Res., vol. 190, p. 106553, Jan. 2021, doi: 10.1016/j.epsr.2020.106553.

[55] P. Saini and S. K. Jain, "A particle swarm optimization for maximum loadability," International Journal of Engineering and Advanced Technology (IJEAT), vol. 2, no. 6, pp. 224–228, Aug. 2013.

[56] A. Chaithra and S. Modi, "Power System Vulnerability Assessment using Voltage Collapse Proximity Index," in 2018 2nd IEEE International Conference on Power Electronics, Intelligent Control and Energy Systems (ICPEICES), Delhi, India: IEEE, Oct. 2018, pp. 39–43. doi: 10.1109/ICPEICES.2018.8897377.

[57] M. Massaoudi, T. Zamzam, M. E. Eddin, A. Ghrayeb, H. Abu-Rub and S. S. Refaat, "Fast Transient Stability Assessment of Power Systems Using Optimized Temporal Convolutional Networks," IEEE Open J. Ind. Appl., vol. 5, pp. 267–282, 2024, doi: 10.1109/OJIA.2024.3426334.

[58] B. Boussahoua and M. Boudour, "Critical Clearing Time Evaluation of Power System with UPFC by Energetic Method," Journal of Electrical Systems, vol. 2009, no. 1, pp. 85–88, Nov. 30, 2009.

[59] X. Liu, H. Xin and D. Chen, "Rotor angle stability analysis and enhancement of Synchronous Condenser in large-scale renewable energy farms," TechRxiv, 2023, doi: 10.36227/techrxiv.20486220.v1.

[60] V. Konoval and R. Prytula, "Participation Factor in Modal Analysis of Power Systems Stability," in Proc. 2020 IEEE 61st Int. Sci. Conf. Power and Electrical Engineering of Riga Technical Univ. (RTUCON), Riga, Latvia, 2020, pp.1–6.doi: 10.1109/RTUCON51174.2020.931660.

Contribution of Individual Authors to the Creation of a Scientific Article (Ghostwriting Policy)

Leeshen Pather carried out the comprehensive research and technical work for the paper, including the study design, literature review, modeling and simulations, data processing, analysis and interpretation of results, preparation of figures and tables, and writing the complete manuscript.

Dr Rudiren Sarma served as the supervisor, providing academic oversight and guidance throughout the project, reviewing the work for technical and scholarly quality and advising on structure, presentation and final revisions.

Sources of Funding for Research Presented in a Scientific Article or Scientific Article Itself

The authors gratefully acknowledge the support and encouragement received from family, colleagues, and the Discipline of Electrical, Electronic and Computer Engineering at the University of KwaZulu-Natal during the preparation of this manuscript.

Conflict of Interest

The authors have no conflicts of interest to declare that are relevant to the content of this article.